Published for SISSA by Springer

Received: *June 4, 2020*
Revised: *September 16, 2020*
Accepted: *September 24, 2020*
Published: *October 30, 2020*

Nuclear modification factors for jet fragmentation

P. Caucal,[a] **E. Iancu,**[a] **A.H. Mueller**[b] **and G. Soyez**[a]

[a] *Institut de Physique Théorique, Université Paris-Saclay, CNRS, CEA, F-91191, Gif-sur-Yvette, France*
[b] *Department of Physics, Columbia University, New York, NY 10027, U.S.A.*

E-mail: paul.caucal@ipht.fr, edmond.iancu@ipht.fr, amh@phys.columbia.edu, gregory.soyez@ipht.fr

Abstract: Using a recently-developed perturbative-QCD approach for jet evolution in a dense quark-gluon plasma, we study the nuclear modification factor for the jet fragmentation function. The qualitative behaviour that we find is in agreement with the respective experimental observations in Pb+Pb collisions at the LHC: a pronounced nuclear enhancement at both ends of the spectrum. Our Monte Carlo simulations are supplemented with analytic estimates which clarify the physical interpretation of the results. The main source of theoretical uncertainty is the sensitivity of our calculations to a low-momentum cutoff which mimics confinement. To reduce this sensitivity, we propose a new observable, which describes the jet fragmentation into subjets and is infrared-and-collinear safe by construction. We present Monte Carlo predictions for the associated nuclear modification factor together with their physical interpretation.

Keywords: Heavy Ion Phenomenology, Jets

ArXiv ePrint: 2005.05852

https://doi.org/10.1007/JHEP10(2020)204

Contents

JHEP10(2020)204

1 Introduction

One important source of information about the dense partonic matter — the *quark-gluon plasma* — created in the intermediate stages of ultrarelativistic heavy ion collisions at RHIC and the LHC comes from studies of jets propagating through this dense medium and of the associated modifications of the jet structure and properties. Generically known as "jet quenching", these modifications cover a large variety of phenomena and observables, from more inclusive ones, like the energy loss by the jet (measured e.g. by the nuclear modification factor R_{AA}), to more detailed ones which probe the pattern of the in-medium jet fragmentation (e.g. jet-substructure observables and the fragmentation function) or the medium response to the jet (which influences the jet shapes).

On the theory side, various approaches and physical scenarios have been proposed. They generally adopt a perturbative QCD (pQCD) picture for the high-virtuality part of the parton showers, but differ in their treatment of the interactions between the jet and the medium, and of the medium itself. Even the approaches assuming a weak QCD coupling throughout most stage do still involve some non-perturbative aspects, like the geometry of the medium and of the interaction region, or the transition from partonic to hadronic degrees of freedom at very low virtualities. Besides, there are several pQCD-based approaches, which differ in their assumptions about the dominant medium effects and the best-suited approximation schemes. Notable differences concern the description of the medium-induced radiation — triggered by the collisions between the partons in the jet and those in the medium — and its interplay with the vacuum-like parton branchings triggered by the virtualities.

It is therefore crucial to identify observables which probe different aspects of the in-medium dynamics and can thus be used to test the physical ingredients and assumptions underlying the various theoretical scenarios. In this paper, we focus on one such observable, the nuclear modification of the jet fragmentation function, for which there are interesting data at the LHC [1], but few dedicated conceptual studies (see however [2–8]). The theoretical framework that we use to address this (and related) observable(s) is the pQCD approach recently developed in refs. [9, 10], in which vacuum-like emissions (VLEs) and medium-induced emissions (MIEs) are factorised from each other via controlled approximations at weak coupling. This simple description is manifestly probabilistic, hence allowing for an efficient Monte-Carlo implementation. In [10], we already successfully applied it to two observables measured at the LHC: the jet R_{AA} (the nuclear modification factor for inclusive jet production) and the z_g-distribution (reflecting the jet substructure in terms of relatively hard splittings).

At a first sight, the fragmentation function looks like an ideal observable to study the jet structure in terms of parton showers and its modifications by the interactions with the medium. Indeed, the experimental results [1] in PbPb collisions at the LHC show an interesting pattern with a strong nuclear enhancement of the jet fragmentation into hadrons visible at both ends of the spectrum, that is, at both small $x \ll 1$ and largish $x \gtrsim 0.5$ (with $x \simeq p_T/p_{T,\text{jet}}$ the longitudinal momentum fraction of a hadron inside the jet.) One should however be cautious as the jet fragmentation function is not a well-defined ("in-

JHEP10(2020)204

frared and collinear safe") quantity in pQCD. This means that its theoretical predictions are strongly sensitive to non-perturbative (confinement) physics like the modelling of the hadronisation mechanism.

Another potential drawback of the fragmentation function, already recognised in the literature [2, 7], is that the nuclear enhancement seen in the LHC data at $x \gtrsim 0.5$ is not necessarily an evidence for new physics in the jet fragmentation at large x, but merely a consequence of the overall energy loss by the jet together with the bias introduced by the initial spectrum for jet production via hard (nucleon-nucleon) scatterings. In that sense, the physics of the in-medium jet fragmentation at large x is strongly correlated with that of the jet R_{AA} — a correlation that we confirm in this paper.

The small-x part of the in-medium fragmentation function is further affected by the fact that, in practice, one cannot distinguish the soft hadrons produced by the fragmentation of the jet itself from those from the medium which are dragged by the wake of the jet and are co-moving with it. This effect, know as the "medium response" should be included in any realistic theoretical comparisons with the data at small x (see e.g. [3–6]). This is however not the case of our current framework in which the medium is simply described as a "brick" with a uniform value for the jet quenching parameter $\hat{q}$, the rate for transverse momentum broadening via elastic collisions. The absence of hadronisation in our framework further limits our accuracy in the small-x region, even though this can to some extend be probed by varying the transverse momentum cut-off of our partonic cascade. In view of these limitations, our current study should be viewed as merely exploratory and we shall not perform a direct comparison between our results and the data [1] for the nuclear modification of the jet fragmentation.

Despite these simplifications, one should still hope that our framework captures (most of) the qualitative features of the nuclear effects on the jet fragmentation and, in particular, those that are mainly driven by the medium effects included in our parton showers. The results for the nuclear modifications of the fragmentation function that we obtain in this paper are indeed encouraging. They show that despite the large uncertainties associated with the poorly-controlled soft-physics effects, one can still use this observable for physical considerations and provide a physical interpretation of some of their dominant qualitative features.

First of all, we find that our Monte Carlo results for the nuclear effects on the jet fragmentation function show the same qualitative behaviour as the respective LHC data [1]. Furthermore, the relative simplicity of our approach allows us to present semi-analytic calculations, based on piecewise approximations, which clarify the physical interpretation of the Monte Carlo results. We are thus able to identify the various physical mechanisms contributing to a given nuclear effect — say, the enhancement in the nuclear fragmentation function at small x — and quantify their relative importance.

Our physical picture at weak coupling includes three main medium-induced phenomena, all originating from multiple elastic collisions off the medium constituents: transverse momentum broadening, medium-induced radiation, and colour decoherence. These phenomena lead to a variety of physical effects. For instance, the energy lost by a jet is associated with soft gluons which, after being produced via medium-induced multiple branchings,

JHEP10(2020)204

are deviated at angles larger than the jet radius by elastic collisions. Vice-versa, the relatively hard medium-induced emissions propagate at small angles, inside the jet, and hence contribute to the final jet multiplicity, both directly and indirectly via their subsequent radiations. The analytic calculations in this paper, supported by numerical tests, show that these phenomena are differently probed by the jet fragmentation at small and large x.

The interplay between the various phenomena is often subtle. For example, one may think that the nuclear enhancement observed in the jet fragmentation function at small x is due to the copious production of soft gluons via medium-induced emissions. This is however not right since the soft gluons produced (via MIEs) inside the medium are efficiently deflected outside the jet by elastic collisions and hence cannot contribute to the jet multiplicity. In reality, the nuclear excess in the jet multiplicity at small x is a combined effect of two phenomena: the colour decoherence, which opens the angular phase-space for radiation outside the medium, and the presence of additional sources for this radiation, as represented by relatively hard, intra-jet, MIEs.

We similarly discuss nuclear effects on the jet fragmentation at large $x \gtrsim 0.5$. This refers to jets which suffer relatively little evolution, so the leading parton is unambiguously identified in the final state. As recognised in the literature [2], these are typically quark-initiated jets, which are less suppressed by the dense medium than the gluon-initiated jets. This argument takes into account the total energy loss by a jet together with the bias introduced by its production spectrum, but it ignores possible nuclear modifications in the fragmentation mechanism itself. To clarify this point, we perform analytic studies of the in-medium jet fragmentation near $x = 1$. We identify several medium effects which compete with each other. Notably, the two MIE effects already mentioned — energy loss at large angles via soft emissions and energy redistribution inside the jet via semi-hard MIEs — act in opposite directions and almost compensate each other, except possibly at $x > 0.9$. We thus conclude that the strong nuclear enhancement seen in the LHC data for the fragmentation function at large $x > 0.5$ is not teaching us much about the jet fragmentation, but only about the jet global energy loss and its interplay with the bias introduced by the steeply-falling initial spectrum.

Although our qualitative description of the LHC data for the jet fragmentation function in Pb+Pb collisions looks satisfactory, it would be still interesting to allow for more precise, quantitative, comparisons between theory and data. Besides the current intrinsic limitations of our approach — which could, at least in principle, be improved in the future —, such comparisons are hindered by the infrared sensitivity of the fragmentation function. Motivated by that, we propose a new, infrared-and-collinear-safe, observable which is directly probing the jet fragmentation. Instead of counting the hadrons inside the jet (in bins of x), this new observable counts the *primary subjets* — i.e. the subjets generated by partons directly emitted by the leading parton — which are *hard enough*, in the sense of having a sufficiently large transverse momentum w.r.t. their emitter. This observable lies on the same footing as other, perhaps more familiar, observables associated with the jet substructure, such as the z_g-distribution. We present our Monte Carlo predictions for this new observables together with their physical interpretation. The associated nuclear effects are rather pronounced and our respective predictions are under control both qualitatively and quantitatively.

JHEP10(2020)204

The paper is organised as follows: in section 2 we provide a brief reminder of our physical picture, introduced in refs. [9, 10]. Section 3 gives our Monte Carlo results for the fragmentation function and discusses the physical mechanisms at play. We give additional details and perform semi-analytic calculations in section 4 for the fragmentation function at large x and in section 5 for small x. Section 6 introduces and discusses our new observable based on subjets and section 7 concludes.

2 General picture and its Monte Carlo implementation

We first provide a brief reminder of the physical picture, and the corresponding implementation as a Monte-Carlo parton shower, as introduced in refs. [9, 10], that we need to discuss our new results on nuclear effects for the fragmentation function.

In essence, our picture includes two types of radiation: standard *vacuum-like emissions* (VLEs) triggered by the parton virtuality, as well as *medium-induced emissions* (MIEs) triggered by collisions between the high-energy partons and the quark-gluon plasma. Our description is correct to double-logarithmic accuracy within perturbative QCD, including running-coupling and hard-collinear (DGLAP-like) branchings for the VLEs. We make the assumption of a fixed (non-expanding) medium of length L. MIEs are treated as multiple BDMPS-Z-like branchings, with a jet-quenching parameter $\hat{q}$ that is fixed in time.

In the double-logarithmic approximation, we have shown [9, 10] that the partonic cascade can be factorised in three steps:

1. a pure vacuum-like cascade with emission *inside the medium*: these corresponds to emissions of angle θ and energy ω satisfying $\omega^3\theta^4 > 2\hat{q}$ and $\theta > \theta_c \equiv \frac{2}{\sqrt{\hat{q}L^3}}$; these emissions have a formation time $t_f = 2/\omega\theta^2$ much smaller than the medium size L;

2. each parton resulting from the above pure-VLE cascade travels through the medium over a distance of order L and can thus source MIEs;

3. the resulting partons (VLEs from the first step and MIEs from the second step) are the source to another cascade of VLEs outside the medium, i.e. in the region $\omega\theta^2 < 2/L$. For each of these cascades, the first emission can occur at any angle (i.e. is not constrained by angular ordering), a consequence of the colour decoherence following the interactions with the medium [11–14].

Our vacuum-like cascade is described as an angular-ordered shower, starting from a maximal angle $\theta_{\max}$ and keeping only emissions with a relative transverse momentum w.r.t. their emitter ($k_\perp = \omega\theta$ for an emission of energy ω at an angle θ) above a cut-off $k_{\perp\min}$. For the third step of the factorised cascade, the first emission can again happen up to angles $\theta_{\max}$.

To the accuracy of interest, the only medium effects on the VLEs occurring inside the medium can be formulated as kinematic boundaries on the (ω, θ) phase-space. This gives a vetoed region for VLEs which is represented pictorially in figure 1. Emissions with $\omega\theta^2 > 2/L$ and $\theta < \theta_c$ are formally produced inside the medium but lose energy coherently

JHEP10(2020)204

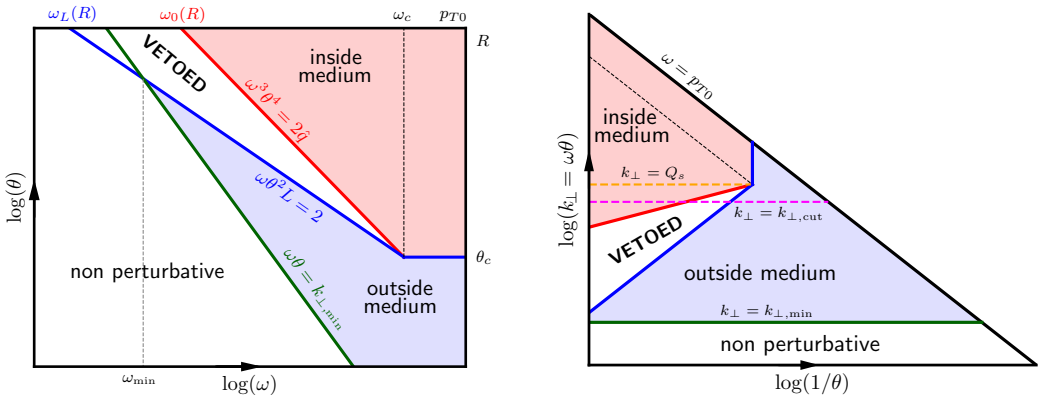

Figure 1. The phase-space for vacuum-like gluon emissions by a jet propagating through a dense QCD medium, in logarithmic units. In the left plot, the variables are the gluon energy ω and its emission angle θ. In the right plot, we rather use the relative transverse momentum $k_\perp \simeq \omega\theta$ and the inverse of the angle $1/\theta$.

with their emitter [11–13]. They can therefore be treated as if they happen outside the medium.

Medium-induced emissions can occur anywhere inside the medium. They are generated with the following emission rate [15–18]:

$$\frac{\mathrm{d}^2\Gamma_{\mathrm{med}}}{\mathrm{d}z\,\mathrm{d}t} = \frac{\alpha_{s,\mathrm{med}}P(z)}{\sqrt{2}\pi}\frac{1}{t_{\mathrm{med}}(x,z)}, \tag{2.1}$$

with $P(z)$ the splitting function and t_{med} the formation time for a MIE off a parent parton with energy xE. Both depend on the partonic channel under consideration. For, say, a $g \to gg$ channel one has

$$t_{\mathrm{med}}(x,z) = \sqrt{\frac{2z(1-z)xE}{[1-z(1-z)]\hat{q}}} \approx \sqrt{\frac{2zxE}{\hat{q}}}, \tag{2.2}$$

where the approximate equality holds for $z \ll 1$. This spectrum is valid for soft emissions, $\omega < \omega_c$, where $\omega = zxE$ is the energy of the emitted gluon and $\omega_c \equiv \hat{q}L^2/2$ is the most energetic such an emission, corresponding to a formation time $t_{\mathrm{med}} = L$. Integrating (2.1) over a time of order L we get the BDMPS-Z spectrum for soft emissions [19–23]

$$\omega\frac{\mathrm{d}\mathcal{P}_{\mathrm{med}}}{\mathrm{d}\omega} = \frac{\alpha_{s,\mathrm{med}}N_c}{\pi}\sqrt{\frac{2\omega_c}{\omega}}\,\Theta(\omega_c-\omega) \tag{2.3}$$

In our Monte Carlo simulations, the QCD coupling $\alpha_{s,\mathrm{med}}$ in eqs. (2.1) and (2.3) is kept fixed.[1]

After being produced at time t, MIEs propagate through the medium over a distance $L-t$ and thus acquire a transverse momentum broadening via random collisions. This is

[1] On physical grounds, one expects that the right momentum scale for the running should be the transverse momentum $k_f^2 = \sqrt{\hat{q}\omega}$ acquired during formation. This energy dependence would complicate the MC implementation.

JHEP10(2020)204

Description	parameters			physics constants		
	$\hat{q}$ [GeV^2/fm]	L [fm]	$\alpha_{s,\mathrm{med}}$	θ_c	ω_c [GeV]	ω_{br} [GeV]
default	1.5	4	0.24	0.0408	60	3.456
similar R_{AA}	1.5	3	0.35	0.0629	33.75	4.134
	2	3	0.29	0.0544	45	3.784
	2	4	0.2	0.0354	80	3.200

Table 1. Table of medium parameters used in this paper. The default set of parameters is given in the first line. The next 3 lines are parameters which give a similar prediction for R_{AA}. The physics scales are defined as $\theta_c = 2/\sqrt{\hat{q}L^3}$, $\omega_c = \hat{q}L^2/2$, and $\omega_{\mathrm{br}} = \bar{\alpha}_s^2\omega_c$, with $\bar{\alpha}_s = \alpha_{s,\mathrm{med}}N_c/\pi$ and $N_c = 3$.

treated as a Gaussian distribution in $k_\perp$, of width $\Delta k_\perp^2 = \hat{q}(L-t)$. A similar broadening applies to the VLEs, for which one can safely take $t \approx 0$ (since $t \sim t_f \ll L$).

Physically, one can identify two main regimes in the cascade of MIEs: `(i)` for $\omega_c \gg \omega \gg \omega_{\mathrm{br}} \equiv (\alpha_{s,\mathrm{med}}N_c/\pi)^2\omega_c$, the probability for multiple emissions is small. This corresponds to relatively rare semi-hard emissions at small angles (in particular at angles which can remain inside a jet). `(ii)` for $\omega \lesssim \omega_{\mathrm{br}}$ multiple branchings are important. This corresponds to a turbulent flow of soft emissions at large angles (larger than the jet radius), which are the main cause for energy loss by the jet [17, 18, 24].

In this picture, the energy lost by a jet is driven by two mechanisms: first, the in-medium vacuum-like cascade creates a sequence of emissions within the jet, then, *each* of these emissions is the source of (soft) MIEs with $\omega \lesssim \omega_{\mathrm{br}}$ which propagate outside the jet. The increase of the number of sources with the jet transverse momentum $p_{T,\mathrm{jet}}$ is crucial for explaining the almost-flat jet nuclear suppression factor R_{AA} observed at high $p_{T,\mathrm{jet}}$ at the LHC [25].

In fine, our Monte-Carlo for parton cascades in the medium contains two "non-physical" parameters: θ_{max} which can be viewed as an uncertainty on our collinear re-summation, and $k_{\perp\mathrm{min}}$ which corresponds to a scale of order Λ_{QCD} (or $\sim 1\,\mathrm{GeV}$) at which hadronisation should become important. It also has 3 "physical" parameters describing the interaction with the medium: $\hat{q}$, L and $\alpha_{s,\mathrm{med}}$. From these 3 parameters one can obtain the constants θ_c and ω_c (which, in particular, control the size of the veto region in figure 1), and ω_{br} which control the energy lost by a parton at large angles (and hence the jet energy loss).

In ref. [10], we found a series of parameters led to a good description of the LHC data for the jet R_{AA}, as measured by ATLAS [25]. These parameters are listed in table 1. It was also shown in [10] that the above picture provides a qualitatively-correct description of the z_g distribution.

Our goal in this paper is to extend our study to the jet fragmentation function. The first set of parameters from table 1 will be our default choice throughout this paper and the other three will be used to probe the sensitivity of the fragmentation function to the medium parameters beyond what is provided by the measurement of R_{AA}.

JHEP10(2020)204

3 Monte Carlo results for the in-medium fragmentation function

In this section, we present our Monte Carlo results for the in-medium modification of the jet fragmentation function together with a discussion of their physical interpretation. This interpretation is supported by the analytic calculations described in the next sections.

3.1 Definitions and general set-up

In order to describe pp and PbPb collisions at the LHC, we consider jets with an initial spectrum given by a pp collision[2] with centre-of-mass energy $\sqrt{s} = 5.02\,\text{TeV}$ computed at leading-order, i.e. with Born-level $2 \to 2$ partonic hard scatterings. A key property of this initial parton (or dijet) spectrum is that it is steeply falling with the partons' transverse momentum p_{T0}: $\mathrm{d}N^{\text{hard}}/\mathrm{d}p_{T0} \propto 1/p_{T0}^n$ with $n \gtrsim 5$. For each event, both final partons are showered using our Monte Carlo. Jets are reconstructed using the anti-$k_\perp$ algorithm [26] as implemented in FastJet v3.3.2 [27]. The final jets are characterised by their transverse momentum $p_{T,\text{jet}}$, which is generally different from the initial momentum p_{T0}, in particular for jets in PbPb collisions which suffer energy loss. The pp baseline is obtained by using the vacuum limit of our Monte Carlo.

We denote the final jet spectrum by $\mathrm{d}N_{\text{jets}}/\mathrm{d}p_{T,\text{jet}}$ and use the upper scripts "med" and "vac" to distinguish between jets in the medium (PbPb collisions) and jets in the vacuum (pp collisions), respectively. The jets can be initiated by either a quark or a gluon. In practice, one often considers the jet yield integrated over an interval in $p_{T,\text{jet}}$, that is,

$$N_{\text{jets}}(p_{T,\text{min}}, p_{T,\text{max}}) = \int_{p_{T,\text{min}}}^{p_{T,\text{max}}} \mathrm{d}p_{T,\text{jet}} \, \frac{\mathrm{d}N_{\text{jets}}}{\mathrm{d}p_{T,\text{jet}}} \,. \tag{3.1}$$

For a given jet with transverse momentum $p_{T,\text{jet}}$, we characterise its fragmentation in terms of the longitudinal momentum fraction

$$x \equiv \frac{p_T \cos(\Delta R)}{p_{T,\text{jet}}}, \tag{3.2}$$

where p_T is the transverse momentum of a constituent of the jet and $\Delta R = \sqrt{(\Delta y)^2 + (\Delta\phi)^2}$, with Δy and $\Delta\phi$ the differences between the jet axis and the particle direction in rapidity and azimuth. Note that since our Monte Carlo does not include hadronisation, the jet constituents are partons.

The jet fragmentation function $\mathcal{D}(x)$ and its nuclear modification factor $\mathcal{R}(x)$ are defined as

$$\mathcal{D}(x) = \frac{1}{N_{\text{jets}}} \frac{\mathrm{d}N}{\mathrm{d}x} \,, \qquad \mathcal{R}(x) = \frac{\mathcal{D}^{\text{med}}(x)}{\mathcal{D}^{\text{vac}}(x)} \,, \tag{3.3}$$

with N_{jets} the number of jets (in the considered $p_{T,\text{jet}}$ range) and $\mathrm{d}N/\mathrm{d}x$ the number of jet constituents with a given momentum fraction x.

[2] For simplicity, we have used the same hard-scattering spectrum for both the pp baseline and the PbPb sample. This means that we neglect the effects of nuclear PDF, which can sometimes be as large as 15-20 % and can be added in a more phenomenologically-oriented study.

JHEP10(2020)204

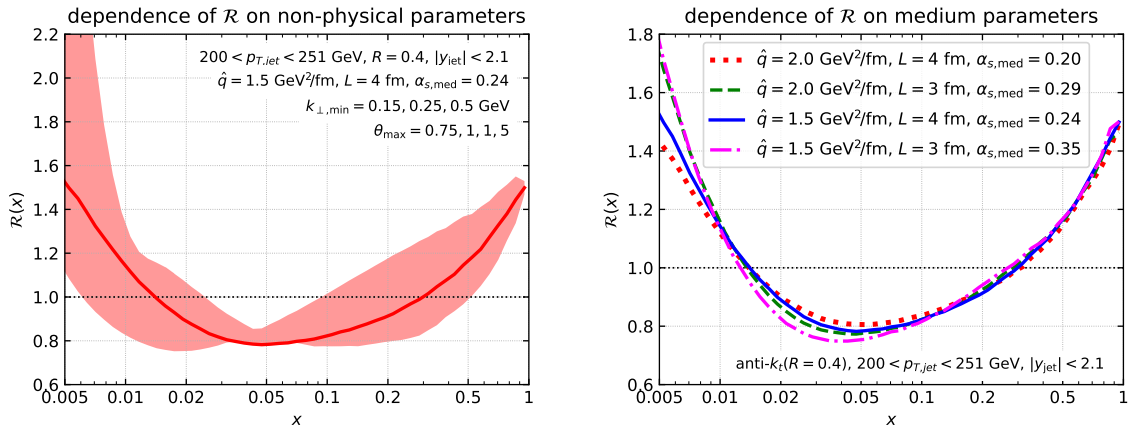

(a) Variations in $\theta_{\max}$ and $k_{\perp,\min}$.

(b) Variations in $\hat{q}$, L and $\alpha_{s,\mathrm{med}}$.

Figure 2. The variability of our MC results for the ratio $\mathcal{R}(x)$ w.r.t. changes in the "unphysical" (left) and "physical" (right) parameters. The 4 sets of values for the "physical" parameters are correlated in that they provide similarly good descriptions of the LHC data [25] for the "standard" nuclear modification factor for jets R_{AA} (see the discussion in [10]).

For later conceptual studies, we shall also consider "monochromatic jets" produced by a well identified parton, quark or gluon, with a fixed initial transverse momentum p_{T0}. In such a case, we denote the fragmentation function by $D_i(x|p_{T0})$, where $i \in \{q, g\}$ refers to the flavour of the leading parton. The corresponding medium/vacuum ratio is defined as $\mathcal{R}_i(x|p_{T0}) \equiv D_i^{\mathrm{med}}(x|p_{T0})/D_i^{\mathrm{vac}}(x|p_{T0})$.

3.2 Monte Carlo results and physical interpretation

We now present our Monte Carlo results for the fragmentation function and the associated nuclear modification factor. We want to pay a special attention to their dependence on the two "unphysical" parameters of the Monte Carlo, $\theta_{\max}$ and $k_{\perp,\min}$, and to the 3 "physical" parameters, $\hat{q}$, L and $\alpha_{s,\mathrm{med}}$. The dependence on the former can be viewed as an uncertainty in our underlying parton-level theoretical description and a large uncertainty would signal a strong dependence of the observable on non-perturbative effects such as hadronisation. Conversely, the dependence on the "physical" medium parameters sheds light on the role and importance of the medium effects at play.

3.2.1 Variability with respect to the unphysical cutoffs

Figure 2(a) displays the sensitivity of our MC results for $\mathcal{R}(x)$ to variations of the "unphysical" parameters around their central values $\theta_{\max} = 1$ and $k_{\perp,\min} = 0.25\,\mathrm{GeV}$, for fixed values of $\hat{q}$, L and $\alpha_{s,\mathrm{med}}$.

The first observation from figure 2(a) is reassuring: the distribution shows a strong enhancement both at small x and at large x, with a nuclear suppression at intermediate values of x. This is in qualitative agreement with experimental measurements (see e.g. [1]).

However, the variations w.r.t. the unphysical parameters appear to be very large. We have checked that they were strongly dominated by variations in $k_{\perp,\min}$. This should not

JHEP10(2020)204

come as a surprise since the fragmentation function, measured directly on individual constituents, is not an infrared-and-collinear (IRC) safe observable. The sizeable variations in the small-x region directly come from the variations of the available phase-space for radiating soft gluons when varying $k_{\perp,\min}$. The large variations in the radiation of soft particles directly affect the spectrum of hard particles in the jet, hence the large uncertainty in the large-x region. Only a proper description of hadronisation (including varying hadronisation parameters) would (hopefully) reduce this uncertainty. This should be kept in mind when studying the dependence of our results on the medium parameters and when comparing our MC results in this work with actual experimental data.

3.2.2 Variability with respect to the (physical) medium parameters

We now fix the unphysical parameters to their central value and study how $\mathcal{R}(x)$ depends on the medium parameters $\hat{q}$, L, and $\alpha_{s,\text{med}}$. We first consider 4 different sets of values, given in table 1 together with the angular and energy scales θ_c, ω_c and ω_{br} characterising the medium-induced radiation, as discussed in section 2.

The plot in figure 2(b) shows our new results for $\mathcal{R}(x)$ for the 4 sets of values for the physical parameters. For large values of x, $x \gtrsim 0.1$, the small variations in ω_{br} (see table 1) are compensated by relatively large variations of ω_c and θ_c. This is similar to what happens for R_{AA}, as discussed at length in ref. [10]. This suggests that for largish $x \gtrsim 0.1$, the nuclear effects on jet fragmentation and on the inclusive jet production are strongly correlated and in particular that they are both controlled by the jet energy loss. Such a correlation has been already pointed out in the literature [2, 7] and used to provide a simple and largely model-independent argument for explaining the enhancement in the ratio $\mathcal{R}(x)$ at $x \gtrsim 0.5$, as observed both in the LHC data [1] and in our MC results in figure 2(b). This argument will be revisited and completed in the next subsection and also in section 4.

Turning to smaller x values, $x \leq 0.01$, the situation becomes different. There is a clear lift of degeneracy between the 4 sets of values, with two of them — corresponding to the smallest medium size $L = 3\,\text{fm}$, but larger values for $\alpha_{s,\text{med}}$ — yielding results that are significantly larger than those predicted by the two other sets (with $L = 4$). In what follows, we provide physical explanations for these trends.

3.3 Behaviour at large x

The behaviour at large x is largely controlled by the physics of energy loss and its interplay with the initial production spectrum, as we now explain.

A jet which, after crossing the medium, is measured with a transverse momentum $p_{T,\text{jet}}$ has originally been produced from a hard quark or gluon emerging from a hard process with a larger momentum $p_{T0} = p_{T,\text{jet}} + \mathcal{E}(p_{T0})$, where $\mathcal{E}(p_{T0})$ is the energy lost by the jet via MIEs at large angles (see ref. [10] for an extensive discussion of this quantity). While the energy lost by a *parton* with momentum $p_T \gg \omega_{\text{br}}$ saturates at a value $\epsilon \sim \omega_{\text{br}}$, which is independent of p_T [17], the average energy lost by a jet keeps increasing with p_{T0}, because

JHEP10(2020)204

of the rise in the phase space for VLEs and hence in the number of partonic sources for medium-induced radiation.[3]

Due to the steeply-falling underlying p_{T0} spectrum, cutting on the jet p_T tends to select jets which lose less energy than average. In particular, this bias favours the "hard-fragmenting" jets which contain a parton with large x (say, $x > 0.5$). Such jets correspond to rare configurations, in which the radiation from leading parton is strongly limited in order to have a final x fraction close to one. Since they contain only few partons, the hard-fragmenting jets suffer very little energy loss, of the order of the partonic energy loss $\epsilon \sim \omega_{\rm br}$. They are therefore less suppressed than the average jets by the steeply-falling initial spectrum. In other terms, the medium acts as a filter which enhances the proportion of hard-fragmenting jets compared to the vacuum.

This bias has already consequences for the *inclusive* jet production, as measured by R_{AA}: the fraction of hard-fragmenting jets among the total number of jets (say, in a given bin in $p_{T,\rm jet}$) is larger in AA collisions than in pp collisions. The effects of this bias are however expected to become even stronger for the jet distribution $\mathrm{d}N/\mathrm{d}x$ at large x, which by definition selects *only* hard-fragmenting jets. This stronger bias towards hard-fragmenting jets has been proposed as an explanation for the nuclear enhancement in the fragmentation function observed in the LHC data [1] at large $x \gtrsim 0.5$. This argument is very general: it applies to a large variety of microscopic pictures for the jet-medium interactions, assuming either weak coupling [5, 28], or strong coupling [29, 30], or a hybrid scenario [3, 7, 8]. All these scenarios naturally predict that hard-fragmenting jets lose less energy towards the medium than average jets, for the physical reason that we already mentioned: hard-fragmenting jets contain less partonic sources for in-medium energy loss. This physical argument is manifest in both the pQCD [5, 28] and the hybrid approaches [3, 7, 8], which explicitly include a vacuum-like parton shower. It is also implicit in the strong coupling scenario in [29, 30] which is tuned such as to reproduce the angular distribution of jets in p+p collisions at the LHC (itself well described by PYTHIA).

In this section, we argue that this is also the main explanation for the rise seen in our results in figure 2(b) at $x \gtrsim 0.5$. Within our pQCD approach this is not entirely obvious since our scenario also allows for nuclear modifications of the fragmentation process itself, via medium-induced emissions and energy loss effects. Similar ingredients are *a priori* present in other scenarios, like JEWEL, but their relative importance has not been explicitly studied to our knowledge. In section 4, we shall perform an extensive study of these effects, via both analytical and numerical (MC) methods. Our conclusions are briefly anticipated towards the end of this section.

Before we discuss the fragmentation function *per se*, let us first demonstrate that, in our picture too, a hard-branching jet loses less energy than the average one. We have numerically verified this, by selecting (in our MC events) jets for which the harder parton carries a momentum fraction $x_{\rm max}$ in a restricted window. These results are presented in figure 3(a) for the energy loss of monochromatic jets and in figure 3(b) for the jet

[3] Within our pQCD picture, this increase in the number of sources for medium-induced emissions explains the fact that R_{AA} increases only slowly with $p_{T,\rm jet}$, including at large $p_{T,\rm jet} \gtrsim 500\,\mathrm{GeV}$ [10].

JHEP10(2020)204

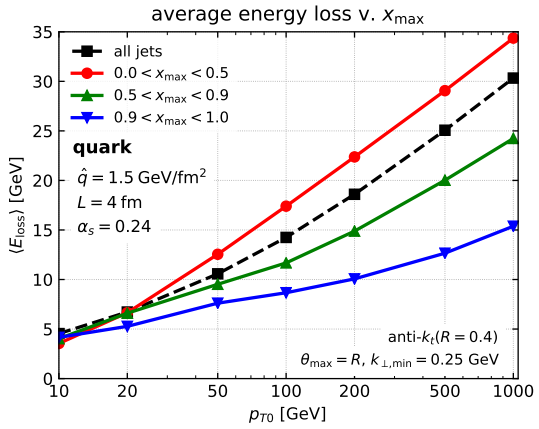

(a) Energy loss as a function of the initial parton transverse momentum p_{T0}.

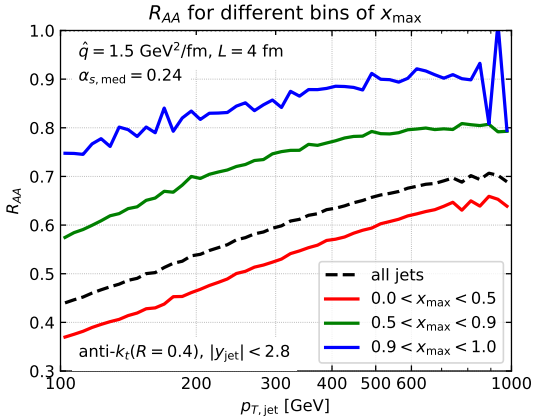

(b) Jet nuclear modification factor R_{AA} as a function of the jet p_T.

Figure 3. Energy loss and R_{AA} for different bins of $x_{\max}$, the momentum fraction of the jet harder constituent.

R_{AA}, for the 3 bins in $x_{\max}$ and (for comparison) also for the inclusive jets. Focusing first on the left figure, we find indeed that the energy lost by jets with $x_{\max} > 0.9$, i.e. hard-fragmenting jets, is both considerably smaller and also less rapidly growing with p_{T0} then for the average jets.[4] As $x_{\max}$ decreases, both the energy loss and its p_{T0} growth increase. This tendency is confirmed by the study of R_{AA}, Figure 3(b), where jets with a large $x_{\max}$ show a smaller-than-average nuclear suppression. It would be interesting to experimentally measure the correlation between the jet R_{AA} and the momentum fraction $x_{\max}$ and compare to our above predictions (see also [7] for a related observable, which compares the nuclear suppression for high-p_T hadrons and inclusive jets).

To have a more quantitative argument, let us focus on a single bin in $p_T \equiv p_{T,\text{jet}}$ with a (vacuum) Born-level p_T spectrum. The vacuum fragmentation function can then be easily estimated as

$$\mathcal{D}^{\text{vac}}(x|p_T) \simeq \frac{N_q(p_T) D_q^{\text{vac}}(x|p_T) + N_g(p_T) D_g^{\text{vac}}(x|p_T)}{N_q(p_T) + N_g(p_T)}\,, \tag{3.4}$$

where $N_i(p_T) \equiv \mathrm{d}N_i^{\text{hard}}/\mathrm{d}p_T \propto 1/p_T^n$ are the initial spectra for quarks ($i = q$) and gluons ($i = g$) and the fragmentation functions for monochromatic jets have been introduced at the end of section 3.1. To write down the corresponding formula for jets in the medium, let us assume that the only medium effect on the jet production is the energy loss. One can thus write

$$\mathcal{D}^{\text{med}}(x|p_T) \simeq \frac{\sum\limits_{i\in\{q,g\}} N_i(p_T + \varepsilon_i(x)) D_i^{\text{med}}(x|p_T + \varepsilon_i(x))}{\sum\limits_{i\in\{q,g\}} N_i(p_T + \mathcal{E}_i(p_T))} \qquad \text{for } x \simeq 1. \tag{3.5}$$

[4] The MC results for $x_{\max} > 0.9$ are only slightly larger than the energy loss expected on the basis of eq. (4.13) for a jet made of two partons. This will play an important role when discussing the large-x behaviour in section 4.

JHEP10(2020)204

The quantity $\varepsilon_i(x)$ in the numerator is the energy loss of a hard-fragmenting jet. It depends on x because the focus on large values $x > 0.5$ selects special configurations in which jets are made with only few partons. Its precise x-dependence is not important for what follows. Rather, it suffices to know that $\varepsilon_i(x)$ is a partonic energy loss, of order $\omega_{\rm br}$, and to a good approximation is independent of the jet p_T. The corresponding quantity in the denominator, $\mathcal{E}_i(p_T)$, is the average energy loss by a jet with transverse momentum p_T. It is much larger than $\varepsilon_i(x)$ and increases with p_T. This difference between the *partonic* energy loss $\varepsilon_i(x)$ in the numerator of eq. (3.5) and the *average* energy loss $\mathcal{E}_i(p_T)$ in its denominator, together with the rapid decrease of $N_i(p_T)$ when increasing p_T, are the origin of the nuclear bias towards hard-fragmenting jets at large x, discussed at the beginning of this section.[5]

On top of their bias towards less energy loss, hard-fragmenting jets also favour quark-initiated jets. There are two reasons for this [2, 10]: `(i)` a quark radiates less than a gluon due to its reduced colour charge ($C_F < C_A$), resulting in a larger probability to contribute at large x, and `(ii)` quark-initiated jets typically contain less partons than gluon-initiated jets and hence lose less energy ($\varepsilon_q < \varepsilon_g$); this feature together with the steeply-falling p_T spectrum favours their production in AA collisions. We can therefore only keep the quark contribution to the numerators of eqs. (3.4) and (3.5) and write

$$\mathcal{R}(x|p_T) \simeq \frac{f_q^{\rm med}(x|p_T)}{f_q^{\rm vac}(p_T)}\,\mathcal{R}_q(x|p_T)\,, \tag{3.6}$$

with the following definitions:

$$f_q^{\rm vac}(p_T) \equiv \frac{N_q(p_T)}{N_q(p_T)+N_g(p_T)}\,, \qquad f_q^{\rm med}(x|p_T) \equiv \frac{N_q(p_T+\varepsilon_q(x))}{\sum\limits_{i\in\{q,g\}} N_i(p_T+\mathcal{E}_i(p_T))}\,. \tag{3.7}$$

For jets in the vacuum, $f_q^{\rm vac}(p_T)$ is simply the fraction of quark-initiated jets. However, the corresponding quantity for jets in the medium is generally *not* a fraction, because of the different energy losses appearing in the numerator and in the denominator of $f_q^{\rm med}(x|p_T)$.

The condition of hard fragmentation ($x \sim 1$) only plays a role in the case of the medium, where it distinguishes between the "partonic" energy loss $\varepsilon_q(x)$ in the numerator and the jet energy loss $\mathcal{E}_q(p_T)$ in the denominator. As already discussed, the physical observation that $\varepsilon_q(x) \ll \mathcal{E}_i(p_T)$ implies that the fraction of hard-fragmenting jets in the medium is larger than that in the vacuum, i.e., $f_q^{\rm med}(x|p_T)/f_q^{\rm vac}(p_T) > 1$, which in turn causes $\mathcal{R}(x|p_T)$ to go above one for $x \lesssim 1$. As x decreases, the energy loss of jets contributing at this value of x increases, becoming closer to $\mathcal{E}(p_T)$ and the nuclear enhancement is less pronounced.

Eq. (3.6) also involves the medium/vacuum ratio $R_q(x|p_T) = D_q^{\rm med}(x|p_T)/D_q^{\rm vac}(x|p_T)$ of the fragmentation functions for quark-initiated, monochromatic, jets. This ratio encodes the nuclear modifications of the fragmentation process itself and is perhaps the most interesting quantity one would like to extract from observables like $\mathcal{R}(x)$ as it encodes internal

[5] Strictly speaking, the "average" energy loss $\mathcal{E}_i(p_T)$ in the denominator is influenced too by this bias, since it should be computed as an average over an inclusive sample of jets produced in AA collisions. However, this bias is less important for the inclusive sample than for the large-x distribution in the numerator of eq. (3.5).

JHEP10(2020)204

properties of the jet rather than its global energy loss. One of the goals of this paper is therefore to identify medium effects on the nuclear modification factor $\mathcal{R}(x)$ beyond global jet energy-loss effects.

Specifically, in section 4 we shall discuss three types of nuclear effects on the fragmentation function $D_q^{\rm med}(x|p_{T0})$, which act in opposite directions and almost compensate each other. First, the presence of a vetoed region in the phase-space for in-medium VLEs reduces the probability for the leading parton to radiate a (vacuum-like) soft gluon and thus increases the probability to find that parton at large x. Then, the energy lost by a two-parton system (after a vacuum-like emission) also goes in this direction.[6] Finally, the MIEs which are hard enough to remain inside the jet (i.e. with energies $\omega > \omega_{\rm br}$) redistribute the energy within the jet and thus decreases the probability to find the leading parton with a fraction x close to one. Our numerical studies show that these effects are individually not so small (at least for x large enough, such that $1 - x \lesssim \omega_c/p_{T0}$), but their net effect on $\mathcal{R}$ is much smaller than the strong enhancement due to the factor $f_q^{\rm med}(x|p_T)/f_q^{\rm vac}(p_T)$.

In summary, for relatively large x, the observable $\mathcal{R}(x)$ is not sensitive to the details of the in-medium fragmentation function, but merely to the bias in the distribution of hard-branching jets as introduced by the deeply falling initial p_T spectrum.

3.4 Behaviour at small x

Let us now consider the situation at small $x \lesssim 0.01$, where our numerical results in figure 2(b) show a pronounced medium enhancement of the fragmentation function, in qualitative agreement with the experimental observations [1]. These results also exhibit a (partial) lift of the degeneracy between the various sets of values for the medium parameters, suggesting a weaker correlation between $\mathcal{R}(x)$ and the jet nuclear modification factor R_{AA}. This section provides explanations for these observations within our framework.

We first note that, for the considered range in $p_{T,\rm jet}$, $x \lesssim 0.01$ corresponds to momenta $p_T \lesssim 2\,\text{GeV}$ for the emitted partons, which are smaller than the characteristic medium scale $\omega_{\rm br}$ for multiple branching. In our framework, such soft emissions are dominated by VLEs outside the medium since MIEs with energies $\omega \lesssim \omega_{\rm br}$ would fragment into very soft gluons propagating at angles larger than the jet radius (i.e. outside the jet). The medium enhancement of VLEs outside the medium has two main origins: `(i)` the violation of angular ordering by the first emission outside the medium, which opens the angular phase-space beyond what is allowed in the vacuum [9, 14], and `(ii)` the presence of MIEs with $\omega > \omega_{\rm br}$ which remain inside the jet and can radiate VLEs outside the medium [10]. Our (analytic and numerical) studies in section 5 show that both effects contribute to explaining the enhancement visible in the MC results.

The above interpretation of the nuclear enhancement at small x as additional VLEs outside the medium does explain the differences between the various choices of medium parameters seen in figure 2(b). A smaller value for L increases the energy phase-space for the parton cascades developing outside the medium because the energy of the first emission outside the medium, $\omega \sim 2/(L\theta^2)$, with an emission angle $\theta \leq R$, increases

[6] A similar effect was discussed in ref. [10] in relation with the z_g distribution.

JHEP10(2020)204

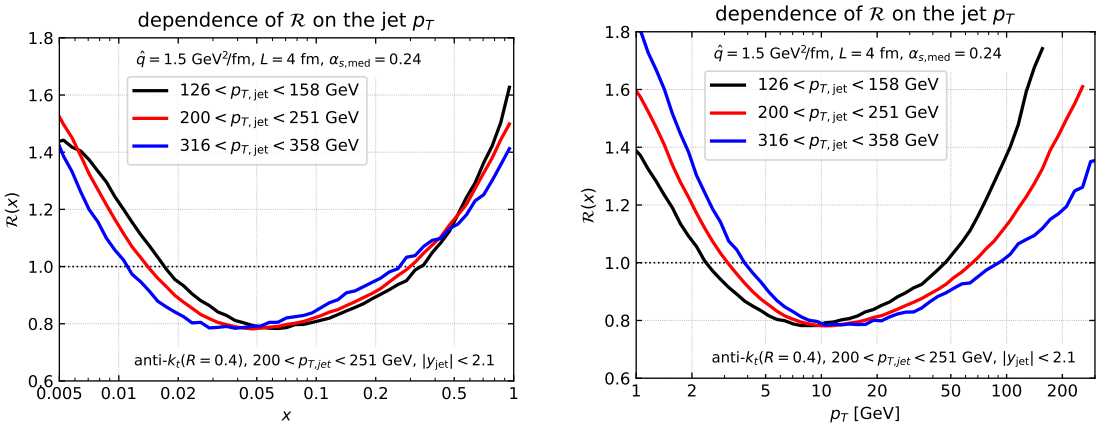

Figure 4. Our MC results for the nuclear modification factor $\mathcal{R}(x)$ shown as a function of the energy fraction x of a jet constituent (left) and of its transverse momentum p_T (right), for 3 bins of the jet $p_{T,\mathrm{jet}}$.

with $1/L$. Furthermore, a larger value of $\alpha_{s,\mathrm{med}}$ enhances the rate for MIEs and hence the number of sources for VLEs outside the medium.

Even though our MC results at small x show the same qualitative trend as the relevant LHC data [1], one must remain cautious when interpreting this agreement. Indeed, our current formalism lacks some important physical ingredients, which are known to influence the soft region of the fragmentation function: the hadronisation and the medium response to the energy and momentum deposited by the jet. Whereas one may expect the effects of hadronisation to at least partially compensate when forming the medium-to-vacuum ratio $\mathcal{R}(x)$, the medium-response effect — i.e. the fact that the experimentally reconstructed jets also include soft particles originating from the wake of moving plasma trailing behind the jet (and not only from the jet itself) — is clearly missing in our approach and its inclusion should further enhance the ratio $\mathcal{R}(x)$ at small x. Indeed, we know from other approaches [3–6], where the medium response is the only (or at least the main) mechanism for producing such an enhancement, that this effect by itself is comparable with the enhancement seen in the data (see also [31] for a different picture).

Of course, it is of utmost importance to complete our formalism with a more realistic description of the medium, including its feedback on the jet. (We shall return to this point in the concluding section.) Before such a more complete calculation is actually performed, it is difficult to anticipate what should be the combined effect of both mechanisms on the behaviour of $\mathcal{R}(x)$ at small x.

3.5 Dependence on the jet p_T

Our Monte Carlo predictions for the nuclear modification $\mathcal{R}(x)$ are shown in figure 4 for three bins of $p_{T,\mathrm{jet}}$ and for the default set of (medium and unphysical) parameters, cf. the first line in table 1. Following the experimental analysis by ATLAS [1], we have separately plotted our results as a function of x (left plot) and of the parton p_T (right plot). The left-hand plot shows only a mild dependence of $\mathcal{R}(x)$ on $p_{T,\mathrm{jet}}$ for $x \gtrsim 0.1$

JHEP10(2020)204

when increasing. In view of eq. (3.6), this suggests a weak $p_{T,\text{jet}}$-dependence for the ratio $f_q^{\text{med}}(x|p_{T,\text{jet}})/f_q^{\text{vac}}(p_{T,\text{jet}})$, which is likely correlated to the similarly weak dependence observed for R_{AA}. At small x, the x scale below which the ratio is larger than 1 decreases with $p_{T,\text{jet}}$, but the corresponding p_T scale increases with $p_{T,\text{jet}}$. These trends are in qualitative agreement with the respective ATLAS results [1].

4 Analytic insight for x close to one

With this section, we start our analytic investigations of the nuclear effects on the jet fragmentation function. Since our main goal is to discuss the effects beyond the jet-spectrum energy-loss factor $f_q^{\text{med}}(x|p_{T,\text{jet}})/f_q^{\text{vac}}(p_{T,\text{jet}})$ in (3.6), we mostly work with monochromatic jets with a given initial transverse momentum p_{T0}. We therefore focus on the jet fragmentation function $D_i(x|p_{T0})$ with $i \in \{q, g\}$, which can be conveniently computed as a derivative of the *cumulative* fragmentation distribution

$$\Sigma_i(x|p_{T0}) \equiv \int_x^1 \mathrm{d}x' D_i(x'|p_{T0})\,. \tag{4.1}$$

We consider separately the two limiting cases where x is either very close to one ($1-x \ll 1$), discussed in this section, or very small ($x \ll 1$), discussed in the next section. For $x \simeq 1$ the integral in the r.h.s. of eq. (4.1) is the probability to find the leading parton with an energy fraction $x' \geq x$.

4.1 Brief summary of the vacuum results

Before addressing the nuclear effects, we briefly recall the main results for jet fragmentation in the vacuum (see e.g. [32]). For simplicity, we identify the jet opening angle R with the maximal angle θ_{max} allowed for the first emission. Due to angular ordering, (most of) the emitted partons will remain inside the jet, hence $p_{T,\text{jet}} = p_{T0}$ and $x = \omega/p_{T0}$, with ω the energy[7] of a parton inside the jet.

When $x \sim 1$, the perturbative expansion of the cumulative fragmentation distribution receives contributions enhanced by two types of logarithms: `(i)` the collinear logarithm $L_0 \equiv \ln(p_{T0}R/k_{\perp,\text{min}})$ generated by integrating over emission angles in the range $k_{\perp,\text{min}}/p_{T0} < \theta < R$, with $k_{\perp,\text{min}}$ the lower transverse-momentum cut-off of the parton shower, and `(ii)` the soft logarithm $L \equiv \ln\frac{1}{1-x}$ generated by integrating over soft gluon emissions with energy fractions z in the range $1-x < z < 1$. The explicit logarithmic dependence on the shower cut-off $k_{\perp,\text{min}}$ is a consequence of the fact that the jet fragmentation function is not IRC-safe. One has $L_0 \geq L$, since all emissions must obey $z\theta p_{T0} > k_{\perp,\text{min}}$ for any $z \geq 1-x$ and any $\theta \leq R$. The resummation of the contributions enhanced by factors L or L_0 can be organised as the following perturbative series

$$\ln(\Sigma_i(x|p_{T0})) = Lg_{1,i}(\alpha_s L, \alpha_s L_0) + g_{2,i}(\alpha_s L, \alpha_s L_0) + O(\alpha_s^{n+1}\ln^n) \tag{4.2}$$

with $\alpha_s \equiv \alpha_s(p_{T0}R) \ll 1$. $Lg_{1,i}$ and $g_{2,i}$ resum respectively all the leading-log (LL) terms $\alpha_s^n \ln^{n+1}$ and the next-to-leading-log (NLL) terms $\alpha_s^n \ln^n$ with $n \geq 1$, where ln means either

[7] We often refer to the transverse momentum p_T of a parton in the jet as its "energy" and use the notation $\omega \equiv p_T$.

JHEP10(2020)204

L, or L_0. We use this perturbative result at NLL accuracy to compute both the vacuum benchmark $D_i^{\rm vac}(x|p_{T0})$ and the contribution of the VLEs to the medium fragmentation function $D_i^{\rm med}(x|p_{T0})$.

The LL piece is the standard double-logarithmic (DL) contribution in which successive emissions are strongly ordered both in energy fraction z and in emission angle θ. It includes the effects of the running of the coupling, $\alpha_s \to \alpha_s(k_\perp)$ with $k_\perp$ the transverse momentum of each emission w.r.t. its emitter, and of the lower momentum cutoff $k_\perp > k_{\perp,\rm min}$. For simplicity and easier physical interpretation of our results, we quote in the main text expressions assuming a fixed coupling. Results including running-coupling effects are presented in appendix. A. All the figures presented in the paper have been obtained using the expressions which include running-coupling effects.

At LL accuracy, one can assume that a single emission, the one with the larger momentum fraction z, dominates the jet fragmentation function near $x = 1$, with all other emissions having much smaller values of z.[8] The probability (4.1) for the leading parton to carry a momentum fraction $x' \geq x$ is the probability for having no emissions with an energy fraction larger than $1 - x$:

$$\Sigma_i^{\rm vac,LL}(x|p_{T0}) = \exp\left(-\frac{2C_i}{\pi}\int_{1-x}^{1}\frac{{\rm d}z}{z}\int_0^R \frac{{\rm d}\theta}{\theta}\alpha_s(k_\perp = z\theta p_{T0})\,\Theta(k_\perp - k_{\perp,\rm min})\right). \tag{4.3}$$

Defining $u \equiv \alpha_0 L$ and $v \equiv \alpha_0 L_0$ $(v > u)$ one easily gets

$$L g_{1,i}^{\rm vac} = \frac{\alpha_s C_i}{\pi}\left[(L_0 - L)^2 - L_0^2\right]. \tag{4.4}$$

which is negative, as expected. The (NLL) calculation of $g_{2,i}$ is more complicated. It is sensitive to multiple emissions and to the non-singular pieces of quark/gluon splitting function. One finds

$$g_{2,i}^{\rm vac} = \gamma_E \frac{\partial L g_{1,i}}{\partial L} - \ln\left[\Gamma\left(1 - \frac{\partial L g_{1,i}}{\partial L}\right)\right] - \frac{2\alpha_s C_i B_i}{\pi} L_0\,, \tag{4.5}$$

with Γ the Euler function, $B_q = \frac{-3}{4}$ and $B_g = -\frac{11CA - 2n_f}{12C_A}$, with n_f the number of active quark flavours. A brief derivation of this expression is given in appendix B.

For gluon jet, we have also included the effect of flavour changes due to $g \to q\bar{q}$ splittings through which the leading parton in a gluon-initiated jet becomes a quark. Although this effect is formally suppressed by powers of $1 - x$ and therefore subleading, it has a sizeable numerical impact. This is because the large Sudakov suppression, eq. (4.4), comes with a factor C_i. A $g \to q\bar{q}$ splittings therefore replaces a suppression enhanced by a factor C_A by one only proportional to C_F, at the expense of a contribution proportional to $\alpha_s(1-x)$ from the splitting itself. This significantly improves our description of the large-x fragmentation of gluon jets in the vacuum and additional details are given in appendix B.

In figure 5, we show the cumulative fragmentation distribution in the vacuum for quark and gluon jets as given by our MC compared to the analytic calculation from eqs. (4.2), (4.4)

[8] At LL, all softer emissions are unresolved by $D_i(x|p_{T0})$ and therefore cancel between real and virtual corrections.

JHEP10(2020)204

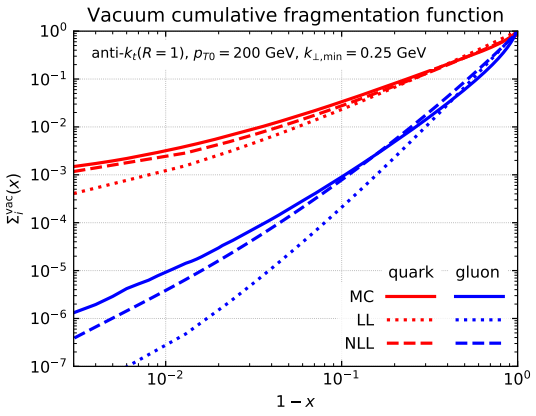

Figure 5. The cumulative fragmentation function $\Sigma_i(x|p_{T0})$ for quark ($i = q$) and gluon ($i = g$) initiated monochromatic jets in the vacuum. Our MC calculations are shown with solid lines, and the two analytic approximations, LL and NLL, by dotted and dashed lines, respectively.

and (4.5). While the LL description captures already the main trend of the distribution, NLL corrections bring a sizeable quantitative improvement. The main conclusion from this figure is that the fragmentation function near $x = 1$ is much larger for quark-initiated jets than for gluon-initiated jets.

4.2 Nuclear effects on the fragmentation function near $x = 1$

To discuss medium-induced effects, it is sufficient to work in the LL approximation where jet fragmentation function near $x = 1$ is dominated by a single, relatively soft, gluon emitted by the leading parton. From this two-parton system we then have to take three effects into account: (1) emissions in the vetoed region of figure 1 are forbidden, (2) the leading parton and the emitted gluon can both lose energy via MIEs at large angles, (3) the gluon emission can be a MIE remaining inside the jet. We consider the effect of the vetoed region before the other two.

4.2.1 Effect of the vetoed region

The effect of the vetoed region in figure 1 can be implemented as a Θ-function excluding this particular region from the phase-space for VLEs. At LL accuracy, this amounts to having an extra factor

$$\Theta_{\rm veto} = 1 - \Theta(\sqrt{2\hat{q}zp_{T0}} - k_\perp^2)\Theta(k_\perp - 2zp_{T0}L^{-1}), \tag{4.6}$$

in the integrand of (4.3). The first (second) Θ-function in the r.h.s. of (4.6) corresponds to the upper (lower) boundary of the vetoed region. For a fixed-coupling approximation, we find assuming for simplicity $1 - x \leq 2/(Lp_{T0}R^2)$ (see appendix A for the result including running coupling)

$$Lg_{1,i}^{\rm veto}(\alpha_s L, \alpha_s L_0) = Lg_{1,i}^{\rm vac}(\alpha_s L, \alpha_s L_0) + \frac{2\alpha_s C_i}{3\pi} \ln^2 \frac{R}{\theta_c}\,. \tag{4.7}$$

JHEP10(2020)204

NLL corrections, $g_{2,i}^{\text{veto}}$, can be obtained using (4.5). In particular, the hard-collinear term proportional to B_i is not modified by the veto region and therefore cancels in the medium/vacuum ratio.

Our analytic estimate for the ratio $R_i(x|p_{T0})$ is shown in figure 6(a) left in green for $p_{T0} = 200\,\text{GeV}$. For comparison, we also show the corresponding MC result, which only includes VLEs (the green curve in figure 6(b)). These results agree well with each other and they both predict a nuclear enhancement near $x = 1$. This enhancement can be easily understood on the basis of (4.7), which implies

$$\ln \frac{\Sigma_i^{\text{veto,LL}}(x)}{\Sigma_i^{\text{vac,LL}}(x)} = \frac{2\alpha_0 C_i}{3\pi} \ln^2 \frac{R}{\theta_c} > 0\,, \tag{4.8}$$

meaning $\Sigma_i^{\text{med}}(x) \simeq \Sigma_i^{\text{veto}}(x) > \Sigma_i^{\text{vac}}(x)$ and hence $R_i(x) > 1$ when $x \to 1$. Indeed, the presence of the vetoed region reduces the phase-space allowed for the decay of the leading parton.

4.2.2 Effect of medium-induced emissions

The medium-induced emissions (MIEs), as triggered by the interactions with the plasma constituents, affect differently the total jet momentum $p_{T,\text{jet}}$ and the energy ω_{LP} carried by its leading parton. This implies a nuclear modification $\mathcal{R}(x)$ at large $x \equiv \omega_{\text{LP}}/p_{T,\text{jet}}$.

For convenience, we focus on the case where x is not *too* close to one, such that $\omega_{\text{br}}/p_{T0} \ll 1 - x \ll 1$, with $\omega_{\text{br}} \sim \alpha_s^2 \hat{q} L^2$ the characteristic scale for multiple branchings. For jets with $p_T \geq 200\,\text{GeV}$, a phenomenological region $0.80 \lesssim x \lesssim 0.95$ translates into $(1-x)p_{T0} \gtrsim 10\,\text{GeV}$ which is indeed larger than $\omega_{\text{br}} \sim 4\,\text{GeV}$ (cf. table 1).

Within this regime, the medium-induced emissions which control the energy loss by the leading parton are relatively hard, with energies $\omega \gg \omega_{\text{br}}$. Thus, they remain inside the jet and can be accurately computed in the single emission approximation. This situation is similar to the one discussed for jets in the vacuum at double-logarithmic accuracy: the parton distribution near $x = 1$ is controlled by a single intra-jet emission, with an energy of the order of $(1-x)p_{T0}$. This emission can be either vacuum-like, or medium-induced. This "semi-hard" emission is accompanied by an arbitrary number of soft MIEs, with energies $\omega \lesssim \omega_{\text{br}}$, which propagate outside the jet and take energy away from the jet constituents. The in-medium fragmentation function near $x = 1$ can therefore be evaluated as:

$$D_i^{\text{med}}(x|p_{T0}) \simeq \int \mathrm{d}\omega\, \Delta_i^{\text{VLE}}(\omega)\, \Delta_i^{\text{MIE}}(\omega) \left[\frac{\partial \mathcal{P}_{i,\text{vac}}}{\partial \omega} + \frac{\partial \mathcal{P}_{i,\text{med}}}{\partial \omega}\right] \delta\left(x - \frac{p_{T0} - \omega - \varepsilon_i}{p_{T0} - \mathcal{E}_i}\right). \tag{4.9}$$

In this expression, $\partial \mathcal{P}_{i,\text{vac}}/\partial\omega$ is the differential probability for emitting a soft gluon with energy ω at any emission angle θ (with $k_{\perp,\text{min}}/\omega < \theta < R$) and $\Delta_i^{\text{VLE}}(\omega)$ is the Sudakov factor forbidding VLEs with energies larger than ω (including the condition (4.6) for the vetoed region), i.e.

$$\Delta_i^{\text{VLE}}(\omega) = \Sigma^{\text{veto}}\left(1 - \frac{\omega}{p_{T0}}\right) \quad \text{and} \quad \frac{\partial \mathcal{P}_{i,\text{vac}}}{\partial \omega} = \frac{\mathrm{d} \ln \Delta_i^{\text{VLE}}}{\mathrm{d}\omega} \simeq \frac{2\alpha_s C_i}{\pi} \frac{1}{\omega} \ln\left(\frac{\omega R}{k_{\perp,\text{min}}}\right), \tag{4.10}$$

where the second expression for $\partial\mathcal{P}_{i,\mathrm{vac}}/\partial\omega$, shown only for illustration, holds for the case of a fixed coupling α_s and ignores the constraints introduced by the vetoed region.

Furthermore, $\partial\mathcal{P}_{i,\mathrm{med}}/\partial\omega$ and $\Delta_i^{\mathrm{MIE}}(\omega)$ are the corresponding quantities for the semi-hard MIE inside the jet ($\theta_c < \theta < R$). Its energy is restricted to $\bar{\omega} < \omega < \omega_c$, where $\omega_c = \hat{q}L^2/2$ and $\bar{\omega}$ is a cutoff of order ω_{br}, separating between "semi-hard" and "soft" MIEs.[9] In this regime, one can safely use the single emission approximation, i.e. (compare to eq. (2.3))

$$\frac{\partial\mathcal{P}_{i,\mathrm{med}}}{\partial\omega_m} \simeq \frac{\alpha_{s,\mathrm{med}}C_i}{\pi}\sqrt{\frac{2\omega_c}{\omega_m^3}}\,, \qquad \Delta_i^{\mathrm{MIE}}(\omega_m) = \exp\left(-\int_{\omega_m}^{\omega_c}\mathrm{d}\omega\,\frac{\partial\mathcal{P}_{i,\mathrm{med}}}{\partial\omega}\right). \tag{4.11}$$

Next, ε_i and $\mathcal{E}_i$ refer to the energy loss via soft MIEs outside the jet ($\theta > R$), for the leading parton and for the jet as a whole, respectively. Finally, the δ-function in eq. (4.9) encodes the fact that, in our present approximation, the energy of the leading parton is the energy p_{T0} of the parton initiating the jet minus the energy of the semi-hard emission and the partonic energy loss ε_i, while the energy of the jet is $p_{T,\mathrm{jet}} = p_{T0} - \mathcal{E}_i$.

For more clarity, we study separately the two types of medium effects included in eq. (4.9), namely energy loss at large angles and energy redistribution via intra-jet MIEs.

4.2.3 Energy loss at large angles

To study the energy loss effects alone, we temporarily neglect the contribution of the intra-jet MIEs to eq. (4.9), which then simplifies to (with ω_s the energy of the soft VLE)

$$D_i^{\mathrm{med}}(x|p_{T0})\Big|_{\text{e-loss}} = \int\mathrm{d}\omega_s\frac{\partial\mathcal{P}_{i,\mathrm{vac}}}{\partial\omega_s}\,\Delta_i^{\mathrm{VLE}}(\omega_s)\,\delta\left(x - \frac{p_{T0}-\omega_s-\varepsilon_i}{p_{T0}-\mathcal{E}_i}\right). \tag{4.12}$$

In the absence of VLEs, a single parton with initial energy ω_0 loses energy by radiating MIEs at large angles ($\theta \gtrsim \theta_c/\bar{\alpha}_s^2$). This is associated with the "turbulent" component of the medium-induced cascades, associated with very soft partons of energies $\omega \lesssim \omega_{\mathrm{br}}$, which are deflected at large angles via collisions with the plasma. The average energy loss is estimated by [17]

$$\varepsilon_i(\omega_0) = \omega_0\left[1 - \mathrm{e}^{-v_0\omega_{\mathrm{br}}/\omega_0}\right], \qquad \text{with} \quad \omega_{\mathrm{br}} = \left(\frac{\alpha_{s,\mathrm{med}}}{\pi}\right)^2 C_A C_i\,\frac{\hat{q}L^2}{2}\,. \tag{4.13}$$

v_0 is a number which can be either obtained via analytic approximations [15, 17, 24] (e.g. one finds $v_0 \simeq 4.96$ for $\omega_0 < \omega_c$), or extracted from MC calculations. ε_i depends on the flavour index i and on the distance L travelled by the parton through the medium. For energetic partons with $\omega_0 \gg \omega_{\mathrm{br}}$ — the most relevant case here —, this energy loss saturates at a value $\varepsilon_i = v_0\omega_{\mathrm{br}}$ independent of ω_0.

For a full jet, the energy loss receives contributions of the form of eq. (4.13) from both the leading parton (LP) and each of the (vacuum-like or medium-induced) *intra-jet*

[9] The precise value of this cutoff is not important: as we will show below the energy integration is controlled by the δ-function, and since the energy losses are relatively small one roughly has $\omega \simeq (1-x)p_{T0} \gg \bar{\omega} \sim \omega_{\mathrm{br}}$.

JHEP10(2020)204

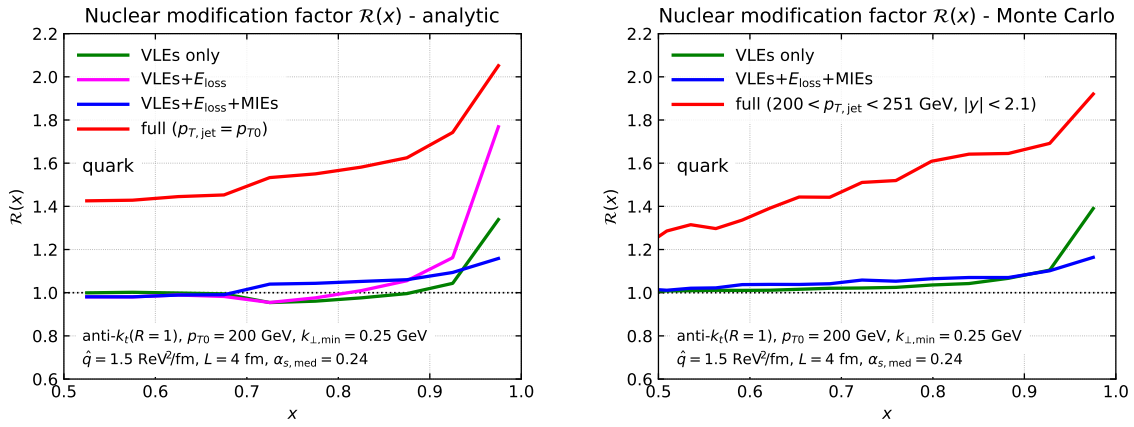

(a) Semi-analytic estimates.

(b) Monte-Carlo simulations.

Figure 6. Nuclear effects on the fragmentation function at large x for monochromatic jets. Three increasingly more physical scenarios are considered: `(i)` VLEs only (only the nuclear effects from the vetoed region are included), `(ii)` adding energy loss via soft MIEs at large angles (not shown on the right plot), and `(iii)` further adding semi-hard MIEs inside the jet. Additionally, we show the "full" curve in red which includes the bias introduced by the initial hard spectrum and is manifestly the dominant effect.

emissions ($\theta < R$) which are radiated within the medium, i.e. in the "inside" region in figure 1. For a hard-fragmenting jet made of only two partons (the LP and a relatively soft VLE, as in eq. (4.12)), we have to consider two options. If the VLE is emitted outside the medium, i.e. either with $\theta < \theta_c$ or with $t_f = 2/(\omega\theta^2) > L$, only the LP loses energy and we have $\mathcal{E}_i = \varepsilon_i$.[10] If the VLE occurs inside the medium, both partons lose energy and we have $\mathcal{E}_i = \varepsilon_i + \varepsilon_g$, with ϵ_g the energy lost by the VLE.[11]

For a VLE inside the medium, the δ-function in eq. (4.12) can be equivalently rewritten as

$$\delta\left(1 - x - \frac{\omega_s - (\mathcal{E}_i - \varepsilon_i)}{p_{T0} - \mathcal{E}_i}\right) \simeq \delta\left(1 - x - z + \frac{(1-z)\mathcal{E}_i - \varepsilon_i}{p_{T0}}\right), \tag{4.14}$$

with $z \equiv \omega_s/p_{T0}$ the splitting fraction of the VLE. We have used the fact that the energy loss is relatively small, $\mathcal{E}_i \ll p_{T0}$. The effect of the in-medium energy loss is a small increase of the splitting fraction, from its initial value in the vacuum, $z_{\text{vac}} = 1 - x$, to

$$z = 1 - x + \frac{(1-z)\mathcal{E}_i - \varepsilon_i}{p_{T0}} \simeq 1 - x + \frac{x\varepsilon_g - (1-x)\varepsilon_i}{p_{T0}} \simeq 1 - x + \frac{\varepsilon_g}{p_{T0}} > z_{\text{vac}}. \tag{4.15}$$

In the second equality we have used $\mathcal{E}_i = \varepsilon_i + \varepsilon_g$ and $z \simeq 1 - x$. For the third equality we have used $x \simeq 1$ and $\varepsilon_g \geq \varepsilon_i$, making clear that the dominant effect is the energy loss by the soft gluon.[12]

[10] For $\theta < \theta_c$, the two partons lose energy coherently, so one can see the energy loss as coming only from the LP [11–13, 33].

[11] In this case, $t_f \ll L$ so the VLE travels a length or order L through the medium.

[12] Interestingly, for a VLE outside the medium (cf. figure 1), we can set $\varepsilon_g \to 0$ to get $z = 1 - x - (1 - x)\varepsilon_i/p_{T0}$ with $1 - x \ll 1$. The energy loss effect is therefore much smaller than for an in-medium VLE and with an opposite sign.

JHEP10(2020)204

The fact that $z > z_{\rm vac} \equiv 1 - x$ means that the probability $P(z) \propto 1/z$ of its emission is smaller, so there is an *enhancement* in the probability for the leading parton to survive at large x. This effect is reinforced by the associated Sudakov factor: when $\omega_s = z p_{T0} > (1-x) p_{T0}$, there is a reduction in the phase-space for emissions by the leading parton and therefore $\Delta_i^{\rm VLE}(\omega_s) > \Delta_i^{\rm VLE}((1-x)p_{T0})$.

The purple curve in figure 6-left shows a calculation of $\mathcal{R}_q(x|p_{T0})$ based on eq. (4.12) together with $\mathcal{E}_q = \varepsilon_q + \varepsilon_g$ and with eq. (4.13) for the partonic energy loss. Compared to the green curve in the same figure, which includes solely the effect of the vetoed region, the purple curves indeed shows a larger enhancement near $x = 1$.

4.2.4 Energy redistribution via a hard MIE

A semi-hard MIE with energy $\omega \gg \omega_{\rm br}$ and which remains inside the jet can modify the fragmentation function $D_i^{\rm med}(x|p_{T0})$ near $x = 1$ in two ways. On one hand, it brings a positive contribution via the term proportional to $\partial \mathcal{P}_{i,\rm med}/\partial\omega$ in eq. (4.9). On the other hand, the additional Sudakov factor $\Delta_i^{\rm MIE}(\omega)$ induces an extra suppression. These two effects are competing with each other. It turns out that the second effect is stronger, resulting in a *decrease* of $D_i^{\rm med}(x|p_{T0})$ near $x = 1$ as compared to the vacuum, and hence a decrease of the medium/vacuum ratio $\mathcal{R}_i(x|p_{T0})$.

We can actually estimate these two contributions to eq. (4.9). To that aim, we can neglect the effects of the energy loss at large angles.[13] Using the δ-function to perform the integral over ω we find

$$D_i^{\rm med}(x|p_{T0})\Big|_{\rm MIE} = p_{T0}\left[\frac{\partial \mathcal{P}_{i,\rm vac}}{\partial\omega} + \frac{\partial \mathcal{P}_{i,\rm med}}{\partial\omega}\right] \Delta_i^{\rm VLE}(\omega)\,\Delta_i^{\rm MIE}(\omega)\Big|_{\omega=(1-x)p_{T0}}. \tag{4.16}$$

We need to show that the "medium" Sudakov effect on the VLE (first term in the square bracket) is larger in absolute value than the direct contribution from MIEs (second term in the square bracket):

$$\frac{\partial \mathcal{P}_{i,\rm vac}}{\partial\omega}\left[1 - \Delta_i^{\rm MIE}(\omega)\right] > \frac{\partial \mathcal{P}_{i,\rm med}}{\partial\omega}\,\Delta_i^{\rm MIE}(\omega)\,. \tag{4.17}$$

At leading-order accuracy for the MIE, one can set $\Delta_i^{\rm MIE} \simeq 1$ in the r.h.s. of the above inequality, whereas in the l.h.s. one must also keep the linear term in its Taylor expansion:

$$1 - \Delta_i^{\rm MIE}(\omega) \;\simeq\; \frac{2\alpha_s C_i}{\pi}\sqrt{\frac{2\omega_c}{\omega}}\,. \tag{4.18}$$

Using a fixed-order approximation for the vacuum emission probability (cf. eq. (4.10)), together with eq. (4.11) for the medium-induced, one finds after simple algebra that eq. (4.17) is equivalent to

$$\frac{4\alpha_s C_i}{\pi}\,\ln\left(\frac{(1-x)p_{T0}R}{k_{\perp,\rm min}}\right) \;>\; 1\,. \tag{4.19}$$

This is satisfied both parametrically and numerically under our working assumptions that collinear logarithms are large. For the parameters used in figure 6, namely $p_{T0} = 200\,\text{GeV}$,

[13] Indeed, in this case, the intra-jet MIE is the dominant medium effect, whereas the energy loss at large angles is a subdominant effect since $\mathcal{E}_i \sim \varepsilon_i \sim \omega_{\rm br}$ are much smaller than $\omega \simeq (1-x)p_{T0}$.

JHEP10(2020)204

$R = 1$, and $k_{\perp,\min} = 0.25\,\text{GeV}$, and with $x = 0.9$ and $\alpha_s = 0.3$, one finds that the l.h.s. of eq. (4.19) is about 5.3.

These considerations are confirmed by the explicit numerical integration of eq. (4.9). The blue curve in figure 6(a) includes all the medium effects discussed in this section (the vetoed region, the energy loss at large angles and the effects of semi-hard MIEs). Comparing it to the purple curve which does not include the effects of semi-hard MIEs, we see that the latter reduce the ratio $\mathcal{R}_i(x|p_{T0})$ near $x = 1$, as expected. This plot also shows that the three medium effects appear to be of similar magnitude and to almost compensate each other, leaving only a modest enhancement at $x \gtrsim 0.9$. This pattern is in very good agreement with what we see from our MC simulations, figure 6(b). Whereas the details of this compensation depend on the specific parameters used in our calculation, we have checked using our MC that such a competition between comparable but opposite effects is a relatively robust prediction from our pQCD scenario.

One can view this conclusion as a little bit deceptive since it shows that the fragmentation function has a reduced sensitivity to nuclear effects associated with the internal dynamics of the jets.

4.3 Bias introduced by the steeply falling jet spectrum

In section 3.3 we have argued (see also [2, 7]) that the strong enhancement of $\mathcal{R}(x)$ seen at large x in the ATLAS Pb+Pb data [1] is a consequence of the bias introduced by the steeply-falling jet spectrum, which favours jets which lose only little energy, notably hard-fragmenting quark-initiated jets. In this section, we present a more detailed (numerical) argument, based on simple 2-parton jets, which supports eq. (3.6) proposed in section 3.3 to quantify this effect.

Eq. (3.6) relies on the "fraction" $f_i(x|p_T)$ of hard-fragmenting jets with one constituent having an energy of at least xp_T. In practice, we define (cf. eq. (3.7))

$$f_q^{\text{vac}}(p_T) = \frac{\frac{\mathrm{d}\sigma_q}{\mathrm{d}p_T}}{\sum\limits_{i\in\{q,g\}} \frac{\mathrm{d}\sigma_i}{\mathrm{d}p_T}}\,, \qquad f_q^{\text{med}}(x|p_T) = \frac{\frac{\mathrm{d}\sigma_q}{\mathrm{d}p_{T0}}\Big|_{p_T+\mathcal{E}_q^{\text{n=2}}}}{\sum\limits_{i\in\{q,g\}} \frac{\mathrm{d}\sigma_i}{\mathrm{d}p_{T0}}\Big|_{p_T+\mathcal{E}_i(p_{T0})}}\,, \tag{4.20}$$

where $\mathrm{d}\sigma_i/\mathrm{d}p_{T0} \propto p_{T0}^{-n_i}$ is the initial jet spectrum. $n_q = 5$ and $n_g = 5.6$ give a decent description over the kinematic range covered in this paper. $\mathcal{E}_i(p_{T0})$ is the average energy loss by a jet with initial transverse momentum p_{T0} and is numerically extracted from MC simulations [10]. $\mathcal{E}_q^{\text{n=2}}$ is the energy lost by a simple two-parton jet (a leading quark of energy fraction $x \sim 1$ and a relatively soft gluon of energy fraction $1 - x$). The dominant contribution (cf. section 4.2.3) comes from events where the quark and gluon lose energy independently of each other:[14] $\mathcal{E}_q^{\text{n=2}} = \varepsilon_q(xp_{T0}) + \varepsilon_g((1-x)p_{T0})$, with ε_g and ε_q given by eq. (4.13).

By combining eq. (4.20) for the fractions of hard-fragmenting jets with our previous calculations of the ratio $\mathcal{R}_q(x|p_T)$ for monochromatic jets, we can provide a semi-analytic

[14] Strictly speaking, the energy argument of ε_g and ε_q should be zp_{T0} and $(1-z)p_{T0}$, respectively, with z the gluon splitting fraction, cf. eq. (4.15), but to the accuracy of interest one can replace $z \simeq 1 - x$ and $p_{T0} \simeq p_T$.

JHEP10(2020)204

estimate for the physical observable $\mathcal{R}(x|p_T)$ using eq. (3.6). This is shown by the red curve in figure 6(a), that should be compared to the corresponding MC result in figure 6(b). The two red curves are both in good agreement with each other and with the general trend seen in the LHC data [1]. For x very close to 1 (mainly the last bin in our plots), the pattern observed in our MC calculations is a combination of the bias induced by the jet spectrum and of the medium effects on the internal jet dynamics $\mathcal{R}_q(x|p_T)$, with a strong domination of the former. The current experimental uncertainties in this region of x are too large to draw a stronger conclusion, notably concerning the relative importance of the nuclear effects associated with $\mathcal{R}_q(x|p_T)$, i.e. with the medium modifications of jet fragmentation itself.

5 Small-x enhancement: colour decoherence and medium-induced radiation

We argued in section 3.4 that the nuclear enhancement of the fragmentation function at small-x, $x \lesssim 0.02$, is driven by two main phenomena: `(i)` colour decoherence, which enlarges the angular phase-space for emissions outside the medium, and `(ii)` medium-induced radiation producing additional partonic sources for these outside-medium emissions. This section provides analytic studies backing up this picture. For simplicity we mostly treat VLEs at fixed coupling and in the double-logarithmic approximation (DLA). We then present MC calculations which hold beyond DLA.

5.1 Analytic estimates

Our aim is to compute the double-differential gluon distribution in a jet of initial transverse momentum (or energy) p_{T0}, initial flavour i and radius R

$$T_i(\omega, \theta^2 | p_{T0}, R^2) = \omega\theta^2 \frac{\mathrm{d}^2 N_i}{\mathrm{d}\omega \mathrm{d}\theta^2} \,. \tag{5.1}$$

The fragmentation function can be obtained from T_i by integrating over all the angles in the jet (with $\theta_{\min} = k_{\perp,\min}/\omega$)

$$\omega D_i(\omega, \theta^2 | p_{T0}, R^2) = \int_{\theta^2_{\min}}^{R^2} \frac{\mathrm{d}\theta_1^2}{\theta_1^2} \, T_i(\omega, \theta_1^2 | p_{T0}, R^2) \tag{5.2}$$

Vacuum case. In pQCD, the leading contribution to the multiplicity of soft gluons in a jet comes from double-logarithmic emissions in a fixed-coupling approximation [34], i.e. via successive VLEs in our context [9]. In this limit, successive gluon emissions are strongly ordered in both energy and emission angle and one finds

$$T_i^{\mathrm{vac}}(\omega, \theta^2 | p_{T0}, R^2) = \frac{\alpha_s C_i}{\pi} \, \mathrm{I}_0 \left(2\sqrt{\bar{\alpha}_s \ln \frac{p_{T0}}{\omega} \, \ln \frac{R^2}{\theta^2}} \right) + \omega\theta^2 \delta(p_{T0} - \omega) \delta(R^2 - \theta^2) \tag{5.3}$$

where $\bar{\alpha}_s = \alpha_s C_A/\pi$ and $\mathrm{I}_0(x)$ is the modified Bessel function of rank 0 which increases exponentially for $x \gg 1$. The second term in the r.h.s. represents the leading parton and

JHEP10(2020)204

the first term is associated with subsequent gluon emissions. The vacuum fragmentation function is then found to be

$$\omega D_i^{\text{vac}}(\omega,\theta^2|p_{T0},R^2) = \delta(p_{T0}-\omega) + \frac{C_i}{C_A}\sqrt{\frac{2\bar{\alpha}_s \ln\frac{\omega R}{k_{\perp,\min}}}{\ln\frac{p_{T0}}{\omega}}}\,\mathrm{I}_1\left(2\sqrt{2\bar{\alpha}_s \ln\frac{p_{T0}}{\omega}\,\ln\frac{\omega R}{k_{\perp,\min}}}\right). \tag{5.4}$$

VLEs in the medium. In the presence of the medium, the DLA calculation is modified by two effects [9]: the presence of a vetoed phase-space for VLEs inside the medium (cf. figure 1), and the colour decoherence allowing for the violation of angular ordering by the first emission outside the medium. At DL accuracy, MIEs can be formally neglected and their discussion is postponed to later in this section. It is helpful to split the medium fragmentation function T_i^{med} in two contributions (see [9]):

$$T_i^{\text{med}}(\omega,\theta^2|p_{T0},R^2) = \Theta_{\text{in}}(\omega,\theta^2)T_i^{\text{vac}} + \Theta_{\text{out}}(\omega,\theta^2)T_{i,\text{out}} \tag{5.5}$$

where the step functions $\Theta_{\text{in/out}}$ enforces that an emission (ω,θ^2) belongs to the "inside" or "outside" region, in the sense of figure 1. The first term, $\Theta_{\text{in}}(\omega,\theta^2)T_i^{\text{vac}}$, corresponding to the in-medium contribution, is unmodified compared to the vacuum. The outside-medium, $T_{i,\text{out}}$, contribution can be expressed as the product of a vacuum-like cascade inside the medium, up to an intermediate point (ω_1,θ_1^2), followed by a first emission outside the medium at (ω_2,θ_2^2) (possibly violating angular ordering), and by a standard vacuum cascade from (ω_2,θ_2^2) to the final point (ω,θ^2):

$$\begin{aligned} T_{i,\text{out}}(\omega,\theta^2|p_{T0},R^2) = \bar{\alpha}_s \int_\omega^{p_{T0}} \frac{\mathrm{d}\omega_1}{\omega_1}\int_{\theta_c^2}^{R^2}\frac{\mathrm{d}\theta_1^2}{\theta_1^2}\,\Theta_{\text{in}}(\omega_1,\theta_1^2)\int_\omega^{\omega_1}\frac{\mathrm{d}\omega_2}{\omega_2} \\ \times\int_{\theta^2}^{R^2}\frac{\mathrm{d}\theta_2^2}{\theta_2^2}\,\Theta_{\text{out}}(\omega_2,\theta_2^2)T_i^{\text{vac}}(\omega_1,\theta_1^2|p_{T0},R^2)T_g^{\text{vac}}(\omega,\theta^2|\omega_2,\theta_2^2) \end{aligned} \tag{5.6}$$

The integral over θ_2^2 is not constrained by the angle θ_1^2 of the previous emission due to absence of angular ordering for the first emission outside the medium.

The two angular integrations in eq. (5.6) can be performed analytically (cf. eq. (5.4)). In ref. [9], the remaining energy integrations were performed numerically. To gain more physical intuition, we now develop an analytic approximation, which is valid when both the energy and angular logarithms are larger than $1/\sqrt{\alpha_s}$. We give here the main ingredients of the calculation and defer details to appendix C.

In the limit of interest, the δ contribution to T^{vac} (the second term in (5.3)) can be neglected in both T^{vac} factors in eq. (5.6), the Bessel functions can be approximated by their (exponential) asymptotic behaviour and the integrations can be evaluated in the saddle-point approximation.

For definiteness, let us consider parameters such that $\omega_L(R) < k_{\perp,\min}/R$, meaning that the hadronisation line $\omega\theta = k_{\perp,\min}$ and the medium boundary $\omega_L(\theta) = 2/(L\theta^2)$ intersect at $\omega_{\min} = Lk_{\perp,\min}^2/2$. In practice we are interested in the fragmentation function at energies ω

JHEP10(2020)204

within the range $\omega_{\min} \ll \omega \ll \omega_c$. The saddle points for ω_1 and ω_2 integrals are respectively found to be (see appendix C)

$$\omega_1^\star = \sqrt{\frac{p_{T0}(2\hat{q})^{1/3}}{R^{4/3}}} = \sqrt{p_{T0}\omega_0(R)}\,, \qquad \omega_2^\star = \sqrt{\frac{2\omega}{L\theta^2}} = \sqrt{\omega\omega_L(\theta)}\,, \tag{5.7}$$

with $\omega_0(\theta) \equiv (2\hat{q}/\theta^4)^{1/3}$ such that $\omega_0(R)$ is the lowest possible energy for a VLE inside the medium.

Several conditions are needed for these saddle points to control the energy integrations. First, the integration ranges must be wide enough, $p_{T0} \gg \omega_0(R)$ and $\omega_L(\theta) \gg \omega$, to allow for large enough logarithmic contributions. This translates into the following conditions:

$$\sqrt{\bar{\alpha}_s}\,\ln\frac{p_{T0}}{\omega_0(R)} \gtrsim 1 \qquad \text{and} \qquad \sqrt{\bar{\alpha}_s}\,\ln\frac{\omega_L(\theta)}{\omega} \gtrsim 1\,. \tag{5.8}$$

Second, for $\omega_1^\star$ to be a genuine saddle point, it must remain smaller than ω_c, meaning

$$p_{T0} < \omega_c \left(\frac{R}{\theta_c}\right)^{4/3} = \frac{\hat{q}^{5/3}L^4R^{4/3}}{2^{7/3}}\,. \tag{5.9}$$

When this condition is satisfied[15] (which is always the case for us in practice), the integral over ω_1 is dominated by relatively low-energy emissions with $\omega_0(\theta) < \omega_1 < \omega_c$, i.e. by the triangular region of the "inside medium" phase-space with energies below ω_c, see figure 1.

Third, energy conservation in eq. (5.6) requires $\omega_2^\star \leq \omega_1^\star$ which implies a θ-dependent upper limit on ω. When computing the fragmentation function using eq. (5.2), this condition must be satisfied for all the angles θ that are integrated over, including lower bound $\theta_{\min} = k_{\perp,\min}/\omega$. This defines a critical energy $\omega_{\rm cr}$, obtained for $\theta = \theta_{\min}$, below which the saddle point method works:

$$\omega < \omega_{\rm cr} = \big(p_{T0}\omega_0(R)\omega_{\min}\big)^{1/3} = \left(\frac{p_{T0}Lk_{\perp,\min}^2(2\hat{q})^{1/3}}{2R^{4/3}}\right)^{1/3} = \left(\frac{p_{T0}k_{\perp,\min}^2}{R^2}\right)^{1/3}\left(\frac{R}{\theta_c}\right)^{2/9}. \tag{5.10}$$

When the conditions in eqs. (5.8)–(5.10) are satisfied, the saddle point method gives a meaningful approximation for the double differential gluon distribution in eq. (5.6), which reads (see appendix C)

$$T_{i,\rm out}(\omega,\theta^2|p_{T0},R^2) \simeq \frac{\alpha_s C_i}{4\pi}\exp\left\{\sqrt{\frac{3\bar{\alpha}_s}{2}}\,\ln\frac{p_{T0}}{\omega_0(R)}\right\}\exp\left\{\sqrt{\bar{\alpha}_s}\,\ln\frac{\omega_L(\theta)}{\omega}\right\} \tag{5.11}$$

The first exponential comes from the integrations over θ_1^2 and ω_1, i.e. over the "inside" region, and can be interpreted as the number of partonic sources generated via VLEs. The second exponential represents the number of gluons generated by each of these sources via gluon cascades developing outside the medium. This simple factorisation between the

[15] In the opposite situation, which would occur for sufficiently large p_{T0}, the dominating region in phase-space is the rectangular region at $\omega_c \leq \omega_1 \leq p_{T0}$ and $\theta_c < \theta_1 < R$; see appendix C for details.

JHEP10(2020)204

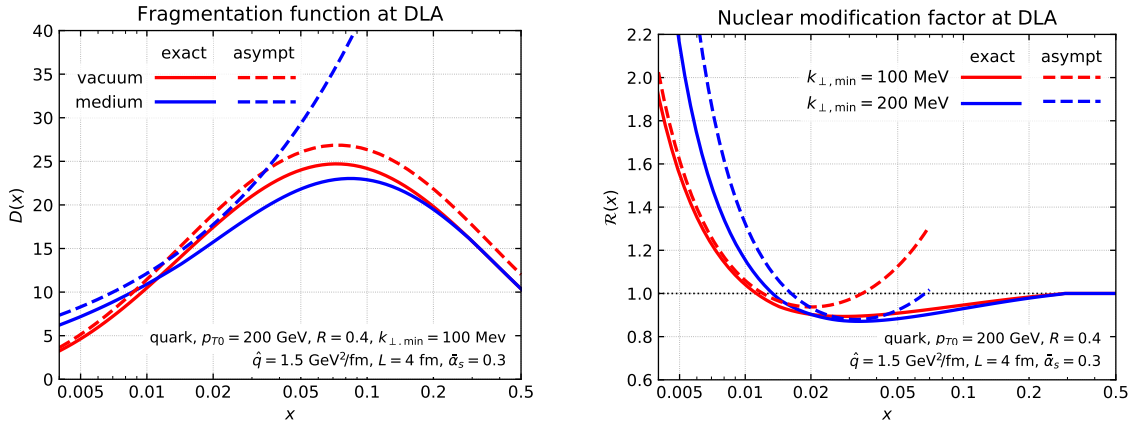

(a) Fragmentation function at DLA

(b) Nuclear modification $\mathcal{R}(x)$ at DLA

Figure 7. Comparison of the exact calculation of fragmentation functions (solid lines) and the asymptotic approximations (dashed lines).

"inside" and the "outside" jet dynamics holds strictly speaking only in the saddle point approximation (and for energies $\omega \leq \omega_{\rm cr}$) and is ultimately a consequence of the colour decoherence which washes out any correlation between the emission angles outside and inside the medium.

Integrating eq. (5.5) over θ using eq. (5.2) we find the fragmentation function for $\omega \leq \omega_{\rm cr}$:[16]

$$\omega D_i^{\rm med}(\omega) \simeq \frac{\sqrt{\bar{\alpha}_s} C_i}{4C_A} \exp\left\{\sqrt{\bar{\alpha}_s}\left(\sqrt{\frac{3}{2}}\ln\frac{p_{T0}R^{4/3}}{(2\hat{q})^{1/3}} + \ln\frac{2\omega}{k_{\perp,\min}^2 L}\right)\right\}. \tag{5.12}$$

The integration is dominated by the lower limit, $\theta = k_{\perp,\min}/\omega$. Since $2\omega/k_{\perp,\min}^2 L = \omega/\omega_{\min} \gg 1$, the second logarithm in (5.12) is positive and $\omega D_i^{\rm med}(\omega)$ decreases when decreasing ω.

Our predictions are shown in figure 7 for the fragmentation function in figure 7(a) and the nuclear modification factor $\mathcal{R}_i(x|p_{T0})$ in figure 7(b). These plots compare the exact results at DLA based on eq. (5.3) and (the numerical integration of) eq. (5.6) for the vacuum and medium results respectively, to their asymptotic counterparts. The latter are obtained by taking the asymptotic behaviour of (5.3) in the vacuum case and by using the saddle-point approximation eq. (5.12) for the medium results. In figure 7(b) we consider two different values for the IR cutoff $k_{\perp,\min}$ (blue: $k_{\perp,\min} = 200\,\text{MeV}$, red: $k_{\perp,\min} = 100\,\text{MeV}$). Overall we see a good agreement, which is moreover improving when $k_{\perp,\min}$ decreases, i.e. when the phase-space increases and the saddle point method becomes more reliable.

The fact that the ratio $\mathcal{R}_i(x|p_{T0})$ increases at small ω can be traced back to angular ordering and the associated humpback plateau [34]. Unlike the double-differential gluon distribution (5.3) which keeps increasing when decreasing ω at fixed θ, the vacuum fragmentation function $\omega D_i^{\rm vac}(\omega)$ in eq. (5.4) develops a maximum at $\omega \simeq \omega_{\rm hump} = (Ek_{\perp,\min}/R)^{1/2}$

[16] The respective contribution of the first term $\propto T_i^{\rm vac}$ in eq. (5.5), that would be non-zero only for $\omega > \omega_0(R)$, is comparatively small, since it lacks the evolution outside the medium.

JHEP10(2020)204

and decreases very fast for ω below $\omega_{\rm hump}$. This is due to the fact that the angular phase-space at $k_{\perp,\rm min}/\omega < \theta < R$ permitted by angular ordering shrinks to zero when decreasing ω. For sufficiently small ω, namely such that[17] $\omega^3 \lesssim p_{T0}k_{\perp,\rm min}^2/R^2$, the denominator $\omega D_i^{\rm vac}(\omega)$ in the medium/vacuum ratio $R_i(x|p_{T0})$ decreases faster with $1/\omega$ than the respective numerator $\omega D_i^{\rm med}(\omega)$ (see also figure 7(a)), so the ratio is increasing.

5.2 Beyond DLA: Monte-Carlo results

In this section we want to extend the DLA arguments from the previous section to include all the ingredients in our physical picture of jet quenching. Our ultimate goal is to provide a deeper understand of the MC results presented in section 3.

For this purpose, it is convenient to think in terms of the factorised picture emerging from our DLA calculation which allows us to write (for $\omega \leq \omega_{\rm cr}$, cf. eq. (5.10))

$$\omega D^{\rm med}(\omega) \simeq \mathcal{N}_{\rm in} \times \left(\omega \frac{{\rm d}N^{\rm out}}{{\rm d}\omega}\right) \tag{5.13}$$

where $\mathcal{N}_{\rm in}$ is the multiplicity of partonic sources produced by the jet evolution inside the medium and $\omega {\rm d}N^{\rm out}/{\rm d}\omega$ is the fragmentation function generated outside the medium by any of these sources. This picture is a consequence of colour decoherence which allows the first out-of-medium emission to be emitted at any angle. This factorisation is not expected to hold beyond DLA, but can still be used for qualitative considerations.

Beyond DLA, several competing expects should be considered. `(i)` VLEs are emitted with the full (DGLAP) splitting functions (including energy conservation) and with a running coupling. These effects are expected to reduce both factors in eq. (5.13). `(ii)` Adding the intra-jet MIEs enhances the multiplicity $\mathcal{N}_{\rm in}$ of the partonic sources. `(iii)` Direct contributions of the MIEs to the fragmentation function $D^{\rm med}(\omega)$ are also possible, but are expected to be a small effect for the jet kinematics ($p_{T0} \sim 200\,{\rm GeV}$, $x \leq 0.02$) and medium parameters (see table. 1) considered in this paper. Indeed, the relevant energies $\omega \lesssim 2\,{\rm GeV}$ are softer than the medium scale $\omega_{\rm br} \sim 4\,{\rm GeV}$ for multiple branching meaning that these MIEs would be deviated outside the jet.

To test these expectations under realistic conditions, we perform MC simulations for inclusive jets (using the full Born-level hard spectrum) with $200 \leq p_T \leq 251\,{\rm GeV}$ and $|y| \leq 2.1$, and with three different scenarios: `(a)` the partons from the hard scattering are showered via VLEs only; `(b)` the partons from the hard scattering are showered via both VLEs and MIEs, but angular ordering is enforced all along the shower, including for the first emission outside the medium (labelled "no decoherence"); `(c)` the physical case where the partons from the hard scattering are showered via both VLEs and MIEs and the angle of the first emission outside the medium is unconstrained.

The MC results for $\mathcal{R}(x)$ are shown in figure 8(a) for each of these three setups. The black curves correspond to setup `(a)` for two 2 different IR cutoffs (solid: $k_{\perp,\rm min} = 200\,{\rm MeV}$, dashed: $k_{\perp,\rm min} = 150\,{\rm MeV}$). compared to the DLA results in figure 7(b) the medium enhancement is strongly reduced and can even be replaced by a suppression for larger values of $k_{\perp,\rm min}$.

[17] The upper limit $p_{T0}k_{\perp,\rm min}^2/R^2$ is smaller than $\omega_{\rm cr}^3$ guaranteeing the validity of the saddle-point method.

JHEP10(2020)204

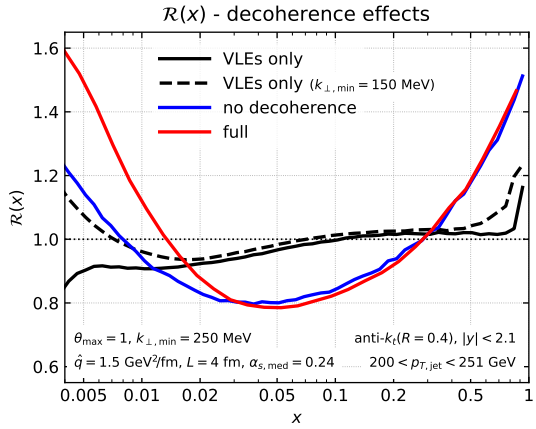

(a) Different physical scenarios: with and without MIEs, and with and without violation of angular ordering.

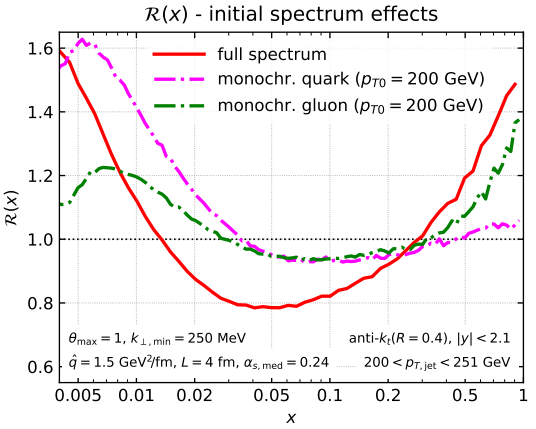

(b) Comparison between quark- and gluon-initiated monochromatic jets and "full" jets including a convolution with the initial, hard spectrum.

Figure 8. Nuclear effects on the fragmentation function at small x. Left figure: 3 different physical scenarios,

Switching on MIEs leads to a robust nuclear enhancement as visible from the blue curve which corresponds to setup `(b)` with $k_{\perp,\min} = 200\,\mathrm{MeV}$. This enhancement is even more pronounced for setup `(c)` corresponding to the red curves in figure 8(a). This new enhancement is easily associated with the fact that the first "outside" emission can be sourced by any "inside" emissions while in setup `(b)` it can only be sourced by "inside" emissions at larger angles.[18] Incidentally, the comparison between the blue and the red curves also shows that the decoherence has no sizeable effects at $x \sim 1$.

For a more detailed understanding, we compare in figure 8(b) the results for $\mathcal{R}(x)$ with the ratio $\mathcal{R}_i(x|p_{T0})$ corresponding to monochromatic jets with $p_{T0} = 200\,\mathrm{GeV}$, for both quark-initiated ($i = q$, magenta, dashed-dotted curve) and gluon-initiated ($i = g$, green, dashed, curve) jets. The small-x enhancement appears to be stronger in the case where the LP is a quark, rather than a gluon. Although this might look surprising at first sight, one should recall that the dominant C_i-dependence for monochromatic jets cancels out in the medium/vacuum ratio $\mathcal{R}_i(x|p_{T0})$. The differences between the quark and gluon curves visible in figure 8(b) is attributed to more subtle sub-leading effects. For example, a gluon jet loses more energy than a quark jet via MIEs at large angles and hence has a (slightly) smaller energy phase-space for radiating outside the medium (and inside the jet).

6 Jet fragmentation into subjets

The fragmentation function defined by eq. (3.3) is not an infrared-and-collinear (IRC) safe observable. It is sensitive to the details of hadronisation which is not included in our

[18] For setup `(b)` the factorisation (5.13) is obviously violated as "inside sources" and "outside emissions" are correlated by angular ordering.

JHEP10(2020)204

present approach. This translates in the strong dependence, observed in figure 2(a), on the cut-off scale $k_{\perp,\min}$ which regulates the infrared behaviour of our partonic cascade. This strong dependence on $k_{\perp,\min}$ is also present in the analytic calculations of sections 4 and 5.

To circumvent this theoretical problem, we propose in this section a different observable which uses subjets instead of individual hadrons to characterise the jet fragmentation. This observable is IRC-safe by construction and is therefore expected to be less sensitive to non-perturbative effects in general and to our $k_{\perp,\min}$ cut-off in particular. There are several ways to define a jet fragmentation function in terms of subjets, e.g. using different jet algorithms or keeping different branches of the clustering tree. The definition we propose below relies on the Cambridge/Aachen algorithm [35, 36]. While other approaches, like those based on the k_t algorithm [37], show a similar behaviour, using the Cambridge/Aachen algorithm appears to be slightly more sensitive to medium effects and easier to study analytically.

6.1 Definition and leading-order estimate in the vacuum

The fragmentation function $\mathcal{D}_{\text{sub}}(z)$ for jet fragmentation into subjets is defined as follows. For a given jet with transverse momentum $p_{T,\text{jet}}$, we iteratively decluster the jet using the Cambridge/Aachen algorithm following the hardest branch (in p_T). At each step, this produces two subjets p_1 and p_2, with $p_{T1} > p_{T2}$. When the relative transverse momentum of the splitting, $k_\perp = p_{T2}\sqrt{\Delta y_{12}^2 + \Delta\phi_{12}^2}$, is larger than a (semi-hard) cut-off $k_{\perp,\text{cut}}$, we compute and record the splitting fraction $z = \frac{p_{T2}}{p_{T1}+p_{T2}}$ of the splitting ($0 < z < 1/2$). The procedure is iterated with the harder branch p_1 until it can no longer be de-clustered. The fragmentation function into subjets is then defined as the density of subjets passing the $k_\perp > k_{\perp,\text{cut}}$ criterion normalised by the total number of jets:[19]

$$\mathcal{D}_{\text{sub}}(z) \equiv \frac{1}{N_{\text{jets}}}\frac{\mathrm{d}N_{\text{sub}}}{\mathrm{d}z} \tag{6.1}$$

The cut-off scale $k_{\perp,\text{cut}}$ regulates the infrared behaviour, guaranteeing that $\mathcal{D}_{\text{sub}}(z)$ be an IRC-safe observable. As long as $k_{\perp,\text{cut}} \gg k_{\perp,\min} \sim \Lambda_{\text{QCD}}$ we therefore expect small non-perturbative effects and a small dependence on the (non-physical) $k_{\perp,\min}$ parameter.

Note that the definition is similar to measuring the Iterated Soft Drop multiplicity [38] differentially in z. It is also directly similar to the primary Lund-plane density [39], $\rho(\theta, k_\perp)$, integrated over all angles θ satisfying the $k_{\perp,\text{cut}}$ condition at fixed $x = k_\perp/(\theta p_{T,\text{jet}})$.

In the soft-and-collinear approximation, corresponding to the double-logarithmic accuracy for $\mathcal{D}_{\text{sub}}(z)$, the vacuum distribution is simply

$$\begin{aligned}\mathcal{D}_{\text{sub}}^{\text{vac}}(z) &\simeq \left[\int_0^R \frac{\mathrm{d}\theta}{\theta}\,\frac{2\alpha_s(z\theta p_{T,\text{jet}})}{\pi z}\Theta(z\theta p_{T,\text{jet}} - k_{\perp,\text{cut}})\right] \times \sum_{i=q,g} C_i\, f_i^{\text{vac}}(p_{T,\text{jet}}),\\ &\overset{\text{f.c.}}{\simeq} \frac{2\alpha_s}{\pi z}\log\left(\frac{zRp_{T,\text{jet}}}{k_{\perp,\text{cut}}}\right) \times \sum_{i=q,g} C_i\, f_i^{\text{vac}}(p_{T,\text{jet}}),\end{aligned} \tag{6.2}$$

[19] We use the notation z for the splitting fraction to emphasise that it is defined w.r.t. the parent subjet, in contrast with the longitudinal momentum fraction x used in the previous sections which is defined as a fraction of the total jet momentum $p_{T,\text{jet}}$.

JHEP10(2020)204

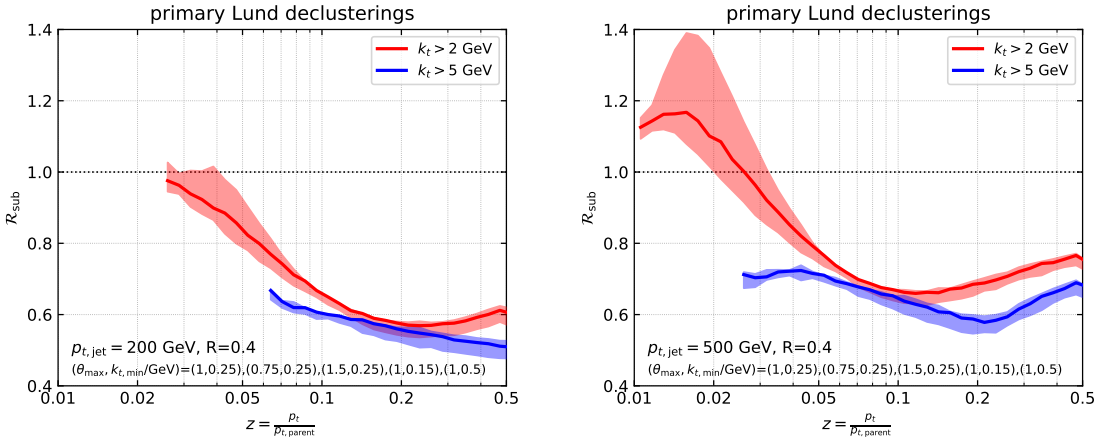

Figure 9. Monte Carlo results for the nuclear modification factor $\mathcal{R}_{\rm sub}(z)$ for the fragmentation function into subjets, for jets with $p_{T,\rm jet} > 200\,\rm GeV$ (left) and $p_{T,\rm jet} > 500\,\rm GeV$ (right) and for 2 values of the lower momentum cut-off $k_{\perp,\rm cut}$ (2 and 5 GeV). The bands show the variability of our results w.r.t. changes in the "unphysical" parameters around their central values $\theta_{\rm max} = 1$ and $k_{\perp,\rm min} = 250\,\rm MeV$.

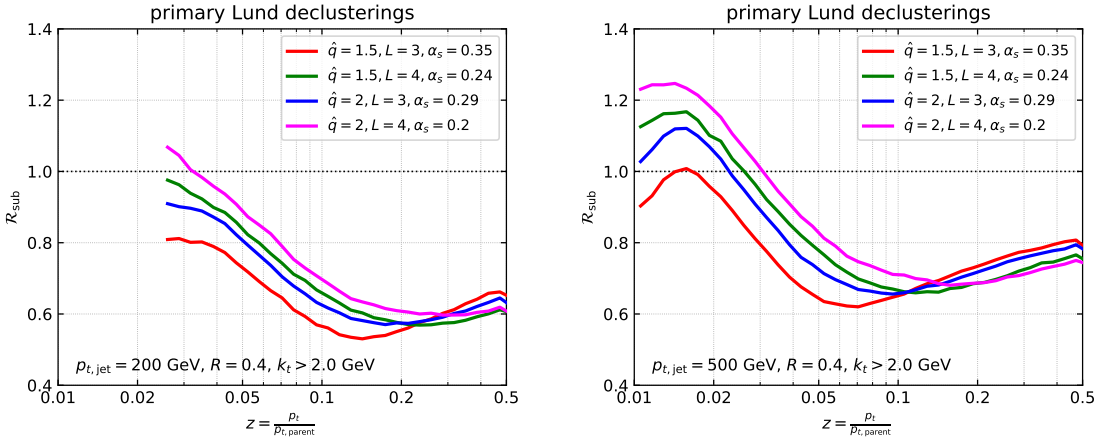

Figure 10. Monte Carlo results for the nuclear modification factor $\mathcal{R}_{\rm sub}(z)$ for the values of the medium parameters that reproduce the ATLAS R_{AA} ratio (cf. figure 2(b)), for the same two ranges in $p_{T,\rm jet}$ as in figure 9 and for $k_{\perp,\rm cut} = 2\,\rm GeV$. The unphysical parameters are fixed to $\theta_{\rm max} = 1$ and $k_{\perp,\rm min} = 250\,\rm MeV$.

where $f^{\rm vac}_{q(g)}(p_{T,\rm jet})$ is the Born-level cross-section for quark (gluon) production with transverse momentum $p_{T,\rm jet}$ normalised to the total number of jets, as defined in eq. (4.20). The second line in the above equation gives the result for a fixed-coupling approximation.

6.2 Nuclear modification for $\mathcal{D}_{\rm sub}(z)$: Monte-Carlo results

In this section, we provide Monte Carlo results for the nuclear modification factor for the fragmentation function into subjets, defined as $\mathcal{R}_{\rm sub}(z) \equiv \mathcal{D}^{\rm med}_{\rm sub}/\mathcal{D}^{\rm vac}_{\rm sub}$.

As for the study of the jet fragmentation function $\mathcal{D}(x)$, we first study the dependence of the the fragmentation function into subjets, $\mathcal{D}_{\rm sub}(z)$, on the non-physical parameters

JHEP10(2020)204

$\theta_{\max}$ and $k_{\perp,\min}$ of our Monte Carlo. This is shown in figure 9 for two different jet p_T cuts (200 and 500 GeV) and two different lower cut-offs $k_{\perp,\text{cut}}$ (2 and 5 GeV). The medium parameters are taken as their default values (cf. table 1) and the non-physical parameters are varied as for figure 2(a). As expected, the uncertainty bands in figure 9 are much smaller than what was observed in figure 2(a), confirming that the (IRC-safe) fragmentation function into subjets $\mathcal{D}_{\text{sub}}(z)$ is under much better perturbative control than (the IRC-unsafe) $\mathcal{D}(x)$.

That said, we must keep in mind that taking $k_{\perp,\text{cut}}$ large-enough to guarantee $k_{\perp,\text{cut}} \gg k_{\perp,\min} \sim \Lambda_{\text{QCD}}$ also cuts some of the medium effects occurring below this cut. E.g., it removes the direct contributions to $\mathcal{D}_{\text{sub}}(z)$ coming from MIEs with transverse momenta $k_\perp \lesssim k_{\perp,\text{cut}}$. One should therefore choose the free parameter $k_{\perp,\text{cut}}$ such as to simultaneously minimise the effects of hadronisation and highlight the interesting medium effects.

In figure 10, we show the subjet fragmentation function for the values of the medium parameters that reproduce the ATLAS R_{AA} ratio (cf. figure 2(b)), for the same two values of $p_{T,\text{jet}}$ as in figure 9 and for $k_{\perp,\text{cut}} = 2\,\text{GeV}$. Compared to figure 2(b), we notice that the curves are less degenerate at small and intermediate values of z. Most importantly, the dependence on the medium parameters is larger than the uncertainty bands related to non-physical parameters shown in figure 9.

6.3 Analytic studies of the nuclear effects

In this section, we would like to disentangle, based on physics considerations and simple analytic calculations, the various nuclear effects contributing to the behaviour observed in the MC results in figure 10. To understand how eq. (6.2) is affected by the medium, it is sufficient to consider jets made of a single splitting (i.e. two subjets) with $k_\perp \geq k_{\perp,\text{cut}}$. For definiteness, all the numerical results shown in this subsection correspond to $k_{\perp,\text{cut}} = 2\,\text{GeV}$.

Vetoed region. When only VLEs are taken into account, the leading medium effect is the vetoed region. Its effect is straightforwardly included in eq. (6.2) by inserting the step-function $\Theta_{\notin\text{veto}}$ defined in eq. (4.6) within the integrand. The largest $k_\perp$ in the vetoed region is $Q_s \equiv (2\hat{q}\omega_c)^{1/4} = (\hat{q}L)^{1/2}$ which is about 2.4 GeV for our default choice of medium parameters. The vetoed region has thus no effect for $k_{\perp,\text{cut}} = 5\,\text{GeV}$ and only a small effect for $k_{\perp,\text{cut}} = 2\,\text{GeV}$ (see figure 1 for an illustration).

This is confirmed both by our analytic calculations, based on eq. (6.2) with the additional constraint $\Theta_{\notin\text{veto}}$, and by MC simulations with only VLEs shown as the black curves in figure 11. Of course, one could enhance the effect of the vetoed region by decreasing the value of $k_{\perp,\text{cut}}$, but this would also amplify the sensitivity of $\mathcal{D}_{\text{sub}}(z)$ to the non-perturbative, soft, emissions.

Incidentally, the previous discussion also shows that, for the ranges of $k_{\perp,\text{cut}}$ considered here, the VLEs which control $\mathcal{D}_{\text{sub}}(z)$ do either occur in the "inside" region of the phase-space in figure 1, or at very small angles $\theta \lesssim \theta_c$ in the "outside" region. They are therefore not significantly affected by colour decoherence. To check that, we have performed MC

JHEP10(2020)204

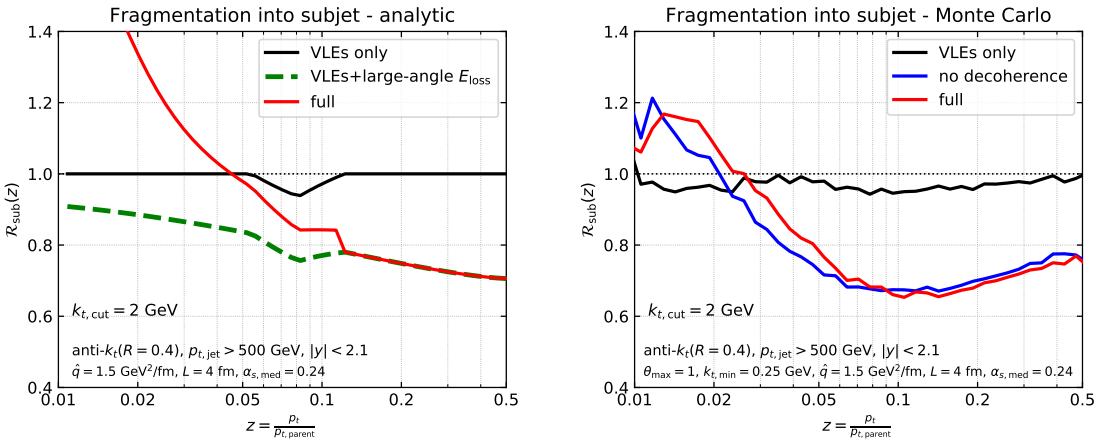

(a) Analytic results

(b) Results from Monte Carlo simulations

Figure 11. Disentangling nuclear effects on the subjet fragmentation function. Left: analytic approximations illustrating the effects of the vetoed region, the energy loss at large angles, and the intra-jet MIEs. Right: MC calculations which illustrate the importance of MIEs and the lack of sensitivity to violations of angular ordering.

calculations with and without the effects of decoherence (i.e. by enforcing or not angular ordering for the first outside emission). The results, shown by the red and blue curves in figure 11(b), respectively, are indeed very close to each other.

Energy loss at large angles. From the discussion in section 4, we already know that the energy loss by a (sub)jet via MIEs at large angles $\theta \gtrsim R$ may have two main effects on a substructure observable such as $\mathcal{D}_{\rm sub}(z)$: `(i)` a shift between the measured value z of the splitting fraction and the respective value at the time of splitting, and `(ii)` a bias introduced by the steeply falling initial spectrum which favours jets losing less energy than average jets, with the second effect being larger than the first one. The same two effects are still at play for $\mathcal{D}_{\rm sub}(z)$. As in the case of the standard fragmentation function discussed in section 4, we expect the effects of the energy loss to be more important for relatively large values $z \gtrsim 0.1$ of the splitting fraction. However, their effects on $\mathcal{R}_{\rm sub}(z)$ is opposite to those on $\mathcal{R}(x)$: unlike the hard-fragmenting jets, which lose *less* energy than the average jets (leading to an enhancement in $\mathcal{R}(x)$ at $x \gtrsim 0.5$), the jets selected by $\mathcal{D}_{\rm sub}(z)$ lose *more* energy than the average jets, so we expect a *nuclear suppression*, $\mathcal{R}_{\rm sub}(z) < 1$, at sufficiently large z. The main reason for this larger energy loss is the following: the jets included in $\mathcal{D}_{\rm sub}(z)$ involve at least two (relatively hard) subjets with $z \gtrsim 0.1$ and $k_\perp > k_{\perp,\rm cut}$. For the typical values of z and $k_\perp$, the angle $\theta \simeq k_\perp/p_{T2}$ between these two subjets is larger than the critical angle θ_c characterising the angular resolution of the plasma ($\theta_c \lesssim 0.06$, see table 1). Accordingly the two subjets lose energy independently from each other and the whole jet loses more energy than a typical jet from the inclusive sample $N_{\rm jets}$ [10, 33] which also includes single-prong jets, as well as two-prong configurations with $\theta < \theta_c$.

This discussion is in qualitative agreement with the MC results in figure 11(b), except at very small z where new effects discussed below contribute. For a more quantitative

JHEP10(2020)204

argument, we notice that, if one neglects the shift in the value of z, then the energy loss at large angles affects only the quark- and gluon-jet "fractions" $f_i^{\rm med}$ in eq. (6.2). These should be computed following eq. (4.20), with different energy losses in the numerator and respectively the denominator. In the numerator, $\mathcal{E}_i^{n=2}$ is the energy loss of jets having two subjets with transverse momentum balance z and angle θ ($p_T \equiv p_{T,\rm jet}$)

$$\mathcal{E}_i^{n=2}(z,\theta) = \mathcal{E}_i((1-z)p_T, R) + \mathcal{E}_g(zp_T, R) \qquad \text{if } (z,\theta) \in \text{ inside region}, \tag{6.3}$$

whereas in the denominator, $\mathcal{E}_i = \mathcal{E}_i(p_T, R)$. Using the energy loss as a function of p_T and R extracted from the MC simulations in ref. [10] in eqs. (4.20) and eq. (6.2), one obtains the dashed, green, curve in figure 11(a). This indeed shows a nuclear suppression, $\mathcal{R}_{\rm sub}(z) < 1$. The suppression is more pronounced at large z, as anticipated, since the discrepancy (in terms of energy loss) between the special jets selected by $\mathcal{D}_{\rm sub}^{\rm med}(z)$ and the average jets increases with z.

Intra-jet MIEs. A relatively hard subjet with $k_\perp > k_{\perp,\rm cut}$ may also be created by a semi-hard MIE, with energy $\omega \gtrsim \omega_{\rm br}$, which remains inside the jet. To leading order, the respective contributions from VLEs and MIEs can be simply added together, as in eq. (4.9). Compared to the latter, the calculation of $\mathcal{D}_{\rm sub}^{\rm med}(z)$ must also keep the information about the emission angle, in order to ensure the condition $k_\perp > k_{\perp,\rm cut}$. We therefore write

$$\mathcal{D}_{\rm sub}^{\rm med}(z) = \left[\int_0^R {\rm d}\theta \left(\frac{2\alpha_s(k_\perp)}{\pi z\theta}\Theta_{\notin \rm veto} + \sqrt{\frac{2\omega_c}{p_{T,\rm jet}}}\frac{\alpha_{s,\rm med}}{\pi z^{3/2}}\mathcal{P}_{\mathcal{B}}(z,\theta)\right)\Theta(k_\perp - k_{\perp,\rm cut})\right] \times \sum_{i=q,g} C_i f_i^{\rm med} \tag{6.4}$$

where $k_\perp = z\theta p_{T,\rm jet}$ and $\mathcal{P}_{\mathcal{B}}(z,\theta) = 2\theta\omega^2\Gamma(0,\omega^2\theta^2/Q_s^2)/Q_s^2$, with $\omega \simeq zp_{T,\rm jet}$ and $Q_s^2 = \hat{q}L$, is the angular distribution due to transverse momentum broadening after emission, averaged over all the emission times between 0 and L [10, 40]. In writing eq. (6.4), we have assumed for simplicity that the energy loss at large angles is given by eq. (6.3) for both the vacuum-like and medium-induced emissions that generates the subjets. This rough approximation could be relaxed in practice, but is sufficient for our illustrative purposes. The distribution $\mathcal{P}_{\mathcal{B}}(z,\theta)$ for MIEs is rather strongly peaked near $k_\perp \sim Q_s$ [10] so its corresponding contribution to eq. (6.4) is expected to be important only when $k_{\perp,\rm cut} \lesssim Q_s$, in which case it should be rapidly increasing at small z. This is in agreement with the MC results in figures 9 and 10, which show an enhancement at small z for $k_{\perp,\rm cut} = 2\,\text{GeV}$ and no visible enhancement for $k_{\perp,\rm cut} = 5\,\text{GeV}$. (Note that Q_s^2 vary between 4.5 and $8\,\text{GeV}^2$ for the different curves shown in these figures.)

Eq. (6.4) includes all the medium effects discussed in this section. The red curve in figure 11(a) shows the result of numerically evaluating the integral in eq. (6.4). The new enhancement at small z compared to the dashed, green, curve is due to the intra-jet MIEs. The overall behaviour agrees well with the full MC results shown in figure 11(b) as well as with figures 9 and 10.

JHEP10(2020)204

7 Conclusions

In this paper, we have studied the fragmentation of a jet propagating through a dense quark-gluon plasma, using a recently-developed pQCD framework in which the vacuum-like and the medium-induced branchings in the parton shower are factorised in time. We have presented both numerical simulations, using a Monte Carlo implementation of our framework, and semi-analytic calculations.

Our main conclusion is that this approach provides a good, qualitative and even semi-quantitative, description for the main nuclear effects observed in the relevant data at the LHC: an enhancement in the jet fragmentation function at both small ($x \ll 1$) and large ($x \gtrsim 0.5$) values for the parton longitudinal momentum fraction $x = p_T/p_{T,\text{jet}}$. This good agreement is obtained for values of the physical parameters that characterise the medium ($\hat{q}$, L and $\alpha_{s,\text{med}}$) which were shown in a previous study to agree with the jet measured nuclear modification factor R_{AA}. Since the fragmentation function is not an infrared-and-collinear-safe quantity in pQCD, our calculations show a strong dependence on the kinematic cutoff $k_{\perp,\text{min}}$ which can be viewed as playing the role of a confinement scale in our (parton-level) framework. Yet, insofar as $k_{\perp,\text{min}}$ is varied within reasonable limits, our result remain in qualitative agreement with the LHC measurements.

The physical interpretation of our results is greatly facilitated by our analytic studies, that we have separately developed using approximations valid either at large x or at small x. These studies have revealed that the nuclear effects visible in the medium/vacuum ratio for the fragmentation function generally involve an interplay between several microscopic phenomena. These phenomena can either change the fragmentation pattern of a "monochromatic" jet (i.e. a jet initiated by a leading parton of a given flavour and energy), or modify the proportion of "monochromatic" jets which contribute to the fragmentation function at a given value of x (within the spectrum of jets produced via hard scattering).

Specifically we have found that the partons contributing to the in-medium fragmentation function at small-x are predominantly produced via VLEs and that their excess w.r.t. the vacuum is the combined result of two mechanisms amplifying each other: the enhanced angular phase-space available to the first emission outside the medium (which, due to the colour decoherence of its emitters, is not constrained by angular ordering) and the additional sources for soft VLEs coming from relatively hard, intra-jet, MIEs. At small-x, the bias introduced by the initial production spectrum, although numerically important, does not alter the overall qualitative behaviour.

The situation at large x, $x \gtrsim 0.5$, is radically different. We have found that the medium effects on the fragmentation function of monochromatic jets, although separately sizeable and physically interesting, act in opposite directions leaving only a small effect on the final result. Their net effect is too small to be distinguished from the significantly larger nuclear enhancement generated by the bias introduced by the initial hard spectrum. This bias favours hard-fragmenting jets initiated by a quark because they lose less energy towards the medium than the average jets. One may be able to avoid, or at least reduce, this bias by looking at rare γ-jet, or Z-jet events (where the energy of the vector boson offers an estimate for the initial energy of the jet) [41, 42], or by using the "quantile" strategy

JHEP10(2020)204

proposed in [43] in the analysis of the nuclear effects on single jets. It would be interesting to check whether such methods could give us a more direct, experimental, access to the genuine modifications in the jet fragmentation function near $x = 1$.

Given the difficulty to make accurate theoretical predictions for a quantity like the jet fragmentation function, which is sensitive to the non-perturbative physics of the confinement, we proposed alternative observables, infrared-and-collinear-safe by construction, which can still be used for studies of the in-medium jet fragmentation. Roughly speaking, these are quantities which characterise the jet fragmentation into subjets where the "subjets" are sufficiently hard to be well within the reach of perturbation theory. We studied one specific example in which the subjets are generated via primary emissions by the leading parton, with a relative transverse momentum larger than a (semi)hard cutoff $k_{\perp,\text{cut}}$. We have shown that by judiciously choosing the value of this cutoff, within the range $k_{\perp,\text{min}} \ll k_{\perp,\text{cut}} < Q_s$, with $Q_s^2 = \hat{q}L$, one can minimise the sensitivity of the results to the infrared cutoff $k_{\perp,\text{min}}$, while still keeping some salient medium effects. It would be interesting to measure this observable at the LHC and compare with our respective predictions in figures 9 and 10.

Whereas the use of infrared-and-collinear-safe observables should strongly reduce the sensitivity of our calculations to the non-perturbative physics of hadronisation, it would be interesting to supplement our framework with a model for hadronisation (both in the vacuum and in the medium) and see how this affects our description of the fragmentation function and its uncertainties.

Finally, the description of the medium in our framework needs to be improved and this is our priority for the future. Notably, we should allow for the longitudinal expansion of the quark-gluon plasma and hence for time-dependent medium parameters. We are currently working on that and our conclusions should hopefully be available in the near future. We are also aiming at an improved theoretical description of the elastic collisions in the plasma and of their consequences in terms of momentum broadening, medium-induced radiation, energy loss and colour decoherence. This should also allow us to include the response of the medium to the jet propagation and thus have a better control on the small-x region of the in-medium fragmentation function and on other observables, like the jet shape and the jet radius (R) dependence of the nuclear modification factor R_{AA} [44–46].

Acknowledgments

The work of P.C., E.I. and G.S. is supported in part by the Agence Nationale de la Recherche project ANR-16-CE31-0019-01. The work of A.H.M. is supported in part by the U.S. Department of Energy Grant # DE-FG02-92ER40699.

A Expressions with running coupling

Several results in this paper have been given in the fixed-coupling approximation. For completeness, we give in this appendix the corresponding results including running coupling effects. These are obtained by evaluating the strong coupling constant at the scale of the

JHEP10(2020)204

transverse momentum $k_\perp$ of each emission with respect to its emitter:

$$\alpha_s(k_\perp) = \frac{\alpha_s}{1 + 2\alpha_s\beta_0 \ln \frac{k_\perp}{p_T R}}, \tag{A.1}$$

with $\alpha_s \equiv \alpha_s(p_T R)$ and $\beta_0 = \frac{11C_A - 2n_f}{12\pi}$.

Defining $u \equiv \alpha_s L$ and $v \equiv \alpha_s L_0$ with $L = \ln \frac{1}{1-x}$ and $L_0 = \ln \frac{p_{T0}R}{k_{\perp,\min}}$ $(v > u)$, the expressions for the NLL Sudakov exponents in the vacuum, eqs. 4.4 and 4.5, become

$$g_{1,i}(u,v) = \frac{C_i}{\pi\beta_0}\left[1 - \ln\left(\frac{1-2\beta_0 u}{1-2\beta_0 v}\right) + \frac{\ln(1-2\beta_0 u)}{2\beta_0 u}\right], \tag{A.2}$$

$$g_{2,i}(u,v) = \gamma_E \frac{\partial u g_{1,i}}{\partial u} - \ln\left[\Gamma\Big(1 - \frac{\partial u g_{1,i}}{\partial u}\Big)\right] + \frac{C_i B_i}{\pi\beta_0}\ln(1-2\beta_0 v)\,, \tag{A.3}$$

The details of the calculation of these functions in the vacuum are given in appendix B.

For the effects of the veto region, the expression corresponding to eq. (4.7) and including running-coupling effects is found to be

$$L g_{1,i}^{\text{veto}}(u,v) = L g_{1,i}(u,v) + \frac{2C_i}{\pi}\mathcal{A}_{\text{veto}}(L) \tag{A.4}$$

where the logarithmic area of the veto region $\mathcal{A}_{\text{veto}}(L)$ is defined as:

$$\mathcal{A}_{\text{veto}}(L) = \int_{e^{-L}}^{1}\frac{\mathrm{d}z}{z}\int_0^R \frac{\mathrm{d}\theta}{\theta}\alpha_s(z p_{T0}\theta)(1-\Theta_{\text{veto}}) \tag{A.5}$$

and Θ_{veto} is given by (4.6). Introducing the following function:

$$\mathcal{T}(x,y,z) \equiv \frac{y+zx}{z}\ln(1+\alpha_s\beta_0(y+zx))\,, \tag{A.6}$$

the logarithmic area $\mathcal{A}_{\text{veto}}(L)$ reads:

$$\begin{aligned}
\mathcal{A}_{\text{veto}}(L) \overset{1-x<z_L}{=}& \frac{1}{2\beta_0}\Big[\mathcal{T}\big(\ln z_0, 0, 2\big) - \mathcal{T}\big(\ln z_L, 0, 2\big) + \mathcal{T}\big(\ln z_c, \tfrac{3}{2}\ln z_0, \tfrac{1}{2}\big) \\
&- \mathcal{T}\big(\ln z_0, \tfrac{3}{2}\ln z_0, \tfrac{1}{2}\big) - \mathcal{T}\big(\ln z_0, \ln z_L, 1\big) + \mathcal{T}\big(\ln z_L, \ln z_L, 1\big) \\
&- \mathcal{T}\big(\ln z_c, \ln z_L, 1\big) + \mathcal{T}\big(\ln z_0, \ln z_L, 1\big)\Big] \\
\overset{z_L<1-x<z_0}{=}& \frac{1}{2\beta_0}\Big[\mathcal{T}\big(\ln z_0, 0, 2\big) - \mathcal{T}\big(-L, 0, 2\big) + \mathcal{T}\big(\ln z_c, \tfrac{3}{2}\ln z_0, \tfrac{1}{2}\big) \\
&- \mathcal{T}\big(\ln z_0, \tfrac{3}{2}\ln z_0, \tfrac{1}{2}\big) - \mathcal{T}\big(\ln z_0, \ln z_L, 1\big) + \mathcal{T}\big(-L, \ln z_L, 1\big) \\
&- \mathcal{T}\big(\ln z_c, \ln z_L, 1\big) + \mathcal{T}\big(\ln z_0, \ln z_L, 1\big)\Big] \\
\overset{z_0<1-x<z_c}{=}& \frac{1}{2\beta_0}\Big[\mathcal{T}\big(\ln z_c, \tfrac{3}{2}\ln z_0, \tfrac{1}{2}\big) - \mathcal{T}\big(-L, \tfrac{3}{2}\ln z_0, \tfrac{1}{2}\big) \\
&- \mathcal{T}\big(\ln z_c, \ln z_L, 1\big) + \mathcal{T}\big(-L, \ln z_L, 1\big)\Big)\Big]
\end{aligned}$$

with $z_0 \equiv \omega_0(R)/p_{T0} = (2\hat{q}/(p_{T0}^3 R^4))^{1/3}$, $z_L \equiv \omega_L(R)/p_{T0} = 2/(L p_{T0} R^2)$ and $z_c \equiv \omega_c/p_{T0}$.

JHEP10(2020)204

B Large x jet fragmentation to NLL accuracy

Eq. (4.5) can be deduced from the coherent branching algorithm (also known as MLLA evolution equation [34]) which resums to all orders leading and next-to-leading logarithms of the form $-\alpha_s \ln(1-x)$. Since the fragmentation function is not IRC safe, we introduce a lower transverse momentum cut-off $k_{\perp,\min}$ for any resolvable splitting. The final result strongly depends on $k_{\perp,\min}$ so we need to keep track of any $k_{\perp,\min}$ dependence in the calculation.

To NLL accuracy, one can neglect the quark/gluon mixing terms. We discuss this approximation at the end of this appendix. We focus on quark-initiated jets and the generalisation to gluon-jets is straightforward. The MLLA equation for the quark cumulative fragmentation function reduces to

$$Q\frac{\partial \Sigma_q(x,Q)}{\partial Q} = \int_0^1 \mathrm{d}z\, K_q^q(z,k_\perp)\left[\Sigma_q\left(\frac{x}{z},zQ\right)-\Sigma_q(x,Q)\right] \tag{B.1}$$

where the evolution variable is $Q = p_{T0}\theta$ to account for the ordering in the angle θ of successive emissions and the kernel is

$$K_q^q(z,k_\perp) = \frac{\alpha_s(k_\perp)}{\pi}P_{qq}(z)\Theta(k_\perp - k_{\perp,\min}), \qquad P_{qq} = C_F\frac{1+z^2}{1-z}. \tag{B.2}$$

The initial condition for (B.1) is $\Sigma_q(x, k_\perp = k_{\perp,\min}) = \Theta(1-x)$. At NLL accuracy, $k_\perp = z(1-z)Q \simeq (1-z)Q$ and $\Sigma_q(\frac{x}{z}, zQ) \simeq \Sigma_q(\frac{x}{z}, Q)$ since the dominant contribution for $x \simeq 1$ comes from $z \simeq 1$.

The standard way to solve eq. (B.1) is to go to Mellin space $\Sigma_q(x,Q) \to \tilde{\Sigma}_q(j,Q)$ where the integral in the r.h.s. becomes a product. In Mellin space, x close to 1 corresponds to $j \to \infty$, more precisely, $\ln(j) \sim -\ln(1-x)$, so we keep all terms of the form $\alpha_s^n \ln(j)^n \sim 1$ in the exact solution. Anticipating our resummed result, we note $\lambda_j = \alpha_s \ln(j)$ and $\lambda_0 = \alpha_s \ln(p_{T0}R/k_{\perp,\min}) = \alpha_s L_0$,

$$\ln(j\tilde{\Sigma}_q(j,p_{T0}R)) = \int_{Q_0}^{p_{T0}R}\frac{\mathrm{d}Q'}{Q'}\int_0^1 \mathrm{d}z\,(z^j-1)K_q^q(z,Q') \tag{B.3}$$

$$\begin{aligned}= \frac{C_F}{\pi\beta_0}\Bigg[\ln(j)\left(1-\ln\left(\frac{1-2\beta_0\lambda_j}{1-2\beta_0\lambda_0}\right)+\frac{\ln(1-2\beta_0\lambda_j)}{2\beta_0\lambda_j}\right)\\ -\gamma_E\ln\left(\frac{1-2\beta_0\lambda_j}{1-2\beta_0\lambda_0}\right)+B_q\ln(1-2\beta_0\lambda_0)\Bigg]+O(\alpha_s\lambda_j^n,\alpha_s\lambda_0^n),\end{aligned} \tag{B.4}$$

where we used the standard trick $z^j - 1 \simeq -\Theta(e^{-\gamma_E}/j - z)$ valid at NLL accuracy [47] and we kept only the singular and finite part $B_q = -3/4$ of the quark splitting function when $z \simeq 1$. Eq. (B.4) resums to all orders leading and next-to-leading logarithms of the form λ_j, λ_0. More explicitly,

$$\ln(j\tilde{\Sigma}_q^{\mathrm{NLL}}(j,p_{T0}R)) = \ln(j)g_1(\lambda_j,\lambda_0)+f_2(\lambda_j,\lambda_0) \tag{B.5}$$

$$g_1(u,v) = \frac{C_F}{\pi\beta_0}\left[1-\ln\left(\frac{1-2\beta_0 u}{1-2\beta_0 v}\right)+\frac{\ln(1-2\beta_0 u)}{2\beta_0 u}\right] \tag{B.6}$$

$$f_{2,q}(u,v) = \frac{C_F}{\pi\beta_0}\left[-\gamma_E\ln\left(\frac{1-2\beta_0 u}{1-2\beta_0 v}\right)+B_q\ln(1-2\beta_0 v)\right] \tag{B.7}$$

JHEP10(2020)204

The final step is to calculate the inverse Mellin transform of (B.4).

$$\Sigma_q(x) = \frac{1}{2\pi i}\int_{\mathcal{C}} \frac{\mathrm{d}j}{j}\, e^{-j\ln(x)}\Big(j\tilde{\Sigma}_q(j)\Big) = \frac{1}{2\pi i}\int_{\mathcal{C}} \mathrm{d}u\, e^{u-\ln(u)+G_q[\ln(u)-\ln(-\ln(x))]} \tag{B.8}$$

where $\mathcal{C}$ is a contour parallel to the imaginary axis and $G_q[\ln(j)] \equiv \ln(j\tilde{\Sigma}_q(j))$. For this, we Taylor-expand the function G_q around $L = -\ln(-\ln(x)) \simeq -\ln(1-x)$.

$$G_q[L+\ln(u)] = G_q[L] + \ln(u)G_q'[L] + \sum_{k=2}^{\infty} \ln(u)^k \frac{G_q^{(k)}[L]}{k!} \tag{B.9}$$

For $k \geq 2$, $G_q^{(k)}[L]$ is certainly beyond NLL accuracy because the derivatives of $\alpha_s\beta_0 L$ with respect to L bring always at least one extra α_s factor. Thus, we truncate the expansion up to the first derivative. Moreover, the derivative of $f_{2,q}(\alpha_s L, \alpha_s L_0)$ with respect to L is also subleading. Finally, using

$$\frac{1}{2\pi i}\int_{\mathcal{C}} \mathrm{d}u\, e^{u+x\ln(u)} = \frac{1}{\Gamma(-x)} \tag{B.10}$$

one gets the following result for the cumulative distribution:

$$\Sigma_q^{\mathrm{NLL}}(x, p_{T0}R) = \frac{e^{G_q[L]}}{\Gamma(1-G_q'[L])} = \frac{\exp\Big(Lg_1(\alpha_s L, \alpha_s L_0) + f_{2,q}(\alpha_s L, \alpha_s L_0)\Big)}{\Gamma\Big(1-\frac{\partial u g_1(u,\alpha_s L_0)}{\partial u}_{|u=\alpha_s L}\Big)} \tag{B.11}$$

which is exactly (4.2), (4.4) and (4.5).

Sub-leading j contributions and quark/gluon mixing terms. Besides N^{2}LL contributions, we have neglected terms of order $\mathcal{O}(\alpha_s^n \ln^n(j)/j)$ in formulas (B.1) and (B.4). Among such terms, those associated with quark/gluon mixings give sizeable numerical corrections to the NLL results, especially in the gluon-jet case. The main reason for this is that, even though the (power-suppressed) probability for a gluon to split in a $q\bar{q}$ pair where the quark carries most of the momentum ($x \sim 1$) is much smaller than the probability to find a hard gluon, once such a splitting occurs, the Sudakov appearing in (B.11) becomes that of a quark, i.e. has a much smaller suppression because of the colour factor $C_F < C_A$ appearing in the exponential. In the inclusive fragmentation function, this becomes an increasingly likely situation [48].

Including all terms of order $O(\alpha_s^n \ln^n(j)/j)$ is beyond the scope of this simple analysis of the large x behaviour of the fragmentation function. Instead, one can correct eq. (B.11) for gluon jets with an additional piece $\Sigma_{g,\mathrm{mix}}(x, p_{T0}R)$ describing the splitting of the gluon in a $q\bar{q}$ pair, with either the quark or the antiquark carrying a large fraction x of the initial energy:

$$\begin{aligned}\Sigma_{g,\mathrm{mix}}(x, p_{T0}R) = &\int_0^{1-x} \mathrm{d}\xi\, P_g^q(\xi) \int_0^R \frac{\mathrm{d}\theta}{\theta}\frac{\alpha_s(\xi p_{T0}\theta)}{\pi}\Theta(\xi p_{T0}\theta - k_{\perp,\min}) \\ &\times \exp\left(-\frac{2C_A}{\pi}\int_\xi^1 \frac{\mathrm{d}z}{z}\int_\theta^R \frac{\mathrm{d}\theta'}{\theta'}\alpha_s(z p_{T0}\theta')\Theta(z p_{T0}\theta' - k_{\perp,\min})\right) \\ &\times \exp\left(-\frac{2C_F}{\pi}\int_\xi^1 \frac{\mathrm{d}z}{z}\int_0^\theta \frac{\mathrm{d}\theta'}{\theta'}\alpha_s(z p_{T0}\theta')\Theta(z p_{T0}\theta' - k_{\perp,\min})\right)\end{aligned} \tag{B.12}$$

JHEP10(2020)204

with $P_g^q(\xi) = 2n_f T_R(\xi^2 + (1-\xi)^2) \simeq 2n_f T_R$ since $\xi \leq 1 - x \ll 1$. In figure 5, the analytical "NLL" curve for gluon jets is actually $\Sigma_g^{\rm NLL}(x) + \Sigma_{g,\rm mix}(x)$.

C Saddle-point method for in-medium intra-jet multiplicity at DLA

Our starting point is eq. (5.6), assuming $\omega_L(R) < k_{\perp,\min}/R$. For definiteness, we also assume $\theta^2 \geq \theta_c^2$, although it turns out that our conclusions remain valid for $\theta^2 \leq \theta_c^2$. It is convenient to use logarithmic variables: $x_1 = \ln(p_{T0}/\omega_1)$, $y_1 = \ln(R^2/\theta_1^2)$, $x_2 = \ln(\omega_2/\omega)$, $y_2 = \ln(\theta_2^2/\theta^2)$ and $X \equiv \ln(p_{T0}/\omega)$, $Y \equiv \ln(R^2/\theta^2)$. The energy scales $\omega_0(R)$ and $\omega_L(R)$, related respectively to the inside and outside domains, become $x_0 \equiv \ln(p_{T0}/\omega_0(R))$ and $x_L \equiv \ln(p_{T0}/\omega_L(R))$, and the logarithmic scale associated with θ_c^2 is $y_c \equiv \ln(R^2/\theta_c^2) = 4(x_L - x_0)/3$. To get the leading asymptotic behaviour of $T_{i,\rm out}(X,Y)$, one can neglect the δ contribution to $T^{\rm vac}$ in (5.3) since it generates terms with at least one exponential factor missing. We thus get

$$T_{i,\rm out}(X,Y) = \bar\alpha_s^3 \int_0^{\min(X,x_0)} dx_1 \int_0^{\min(y_c,\frac{3}{2}(x_0-x_1))} dy_1 \times \int_0^{\min(X-x_1,X+Y-x_L)} dx_2 \int_0^{X+Y-x_L-x_2} dy_2 \mathrm{I}_0(2\sqrt{\bar\alpha_s x_1 y_1})\,\mathrm{I}_0(2\sqrt{\bar\alpha_s x_2 y_2}) \tag{C.1}$$

The integral over y_1 and y_2 can be performed exactly using the the following relation:

$$\int_0^s dy\,\mathrm{I}_0(2\sqrt{\bar\alpha_s x y}) = \sqrt{\frac{s}{\bar\alpha_s x}}\mathrm{I}_1(2\sqrt{\bar\alpha_s x s}) \overset{\bar\alpha_s x s \gg 1}{\simeq} \sqrt{\frac{s}{\bar\alpha_s x}}\frac{\exp(2\sqrt{\bar\alpha_s x s})}{\sqrt{4\pi\sqrt{\bar\alpha_s x s}}}. \tag{C.2}$$

Using (C.2), one gets

$$T_{i,\rm out}(X,Y) = \bar\alpha_s^3 \int_0^{\min(X,x_0)} dx_1 \int_0^{\min(X-x_1,X+Y-x_L)} dx_2\, R_1(x_1) R_2(x_2) \times e^{2\sqrt{\bar\alpha_s x_1 \min(y_c,\frac{3}{2}(x_0-x_1))}} e^{2\sqrt{\bar\alpha_s x_2 (X+Y-x_L-x_2)}} \tag{C.3}$$

with the two non-exponential functions

$$R_1(x_1) = \frac{1}{\sqrt{4\pi}}\frac{(\min(y_c, \frac{3}{2}(x_0-x_1)))^{1/4}}{(\bar\alpha_s x_1)^{3/4}}, \quad R_2(x_2) = \frac{1}{\sqrt{4\pi}}\frac{(X+Y-x_L-x_2)^{1/4}}{(\bar\alpha_s x_2)^{3/4}}. \tag{C.4}$$

The x_2 integrations cannot be performed exactly so we use the saddle-point approximation:

$$\int_{x_1}^{x_2} dx\, f(x) e^{M g(x)} \overset{M\to\infty}{\simeq} \sqrt{\frac{2\pi}{-M g''(x^\star)}} f(x^\star) e^{M g(x^\star)}, \tag{C.5}$$

where the saddle point $x^\star$ is the *maximum* of $g(x)$ between x_1 and x_2. This formula is valid as long as $x_1 < x^\star < x_2$.

JHEP10(2020)204

Setting $M_2 \equiv (X+Y-x_L) = \ln(\omega_L(\theta)/\omega)$ and integrating over x_2/M_2, one get

$$\mathcal{N}_{\rm out} \equiv \bar{\alpha}_s \int_0^{\min(X-x_1, X+Y-x_L)} dx_2\, R_2(x_2) e^{2\sqrt{\bar{\alpha}_s x_2 (X+Y-x_L-x_2)}} \overset{\sqrt{\bar{\alpha}_s} M_2 \to \infty}{\simeq} \frac{1}{2} e^{\sqrt{\bar{\alpha}_s} M_2}. \quad \text{(C.6)}$$

The corresponding saddle point is $x_2^\star = M_2/2 = \ln(\sqrt{\omega_L(\theta)/\omega})$ so that the saddle-point approximation is valid if $x_2^\star < X - x_1$. This gives the condition $x_1 \leq X - x_2^\star$ in the first integral, in order to ensure energy conservation along the cascade.

Calling $\mathcal{N}_{\rm med}$ the remaining integral over x_1, which is truly a gluon multiplicity *inside* the medium, we are left with:

$$\mathcal{N}_{\rm med} \equiv \bar{\alpha}_s \int_0^{\min(x_0, X-x_2^\star)} dx_1\, R_1(x_1) e^{2\sqrt{\bar{\alpha}_s x_1 \min(y_c, \frac{3}{2}(x_0-x_1))}}. \quad \text{(C.7)}$$

Since $\min(X - x_2^\star, x_0) > x_c \equiv \ln(p_{T0}/\omega_c)$, the integral can be split into two pieces: $x_1 < x_c$ where $\min(y_c, 3(x_0-x_1)/2) = y_c$ and $x_1 > x_c$ where $\min(y_c, 3(x_0-x_1)/2) = 3(x_0-x_1)/2$. The first piece is calculated exactly, and we use again the saddle point method to evaluate the second piece, assuming $x_0 = \ln(p_{T0}/\omega_0(R)) \to \infty$. We get (using $x_1' = x_1/x_0$)

$$\begin{aligned}
\mathcal{N}_{\rm med} &= \int_0^{x_c} dx_1 \bar{\alpha}_s \sqrt{\frac{y_c}{\bar{\alpha}_s x_1}} \mathrm{I}_1(2\sqrt{\bar{\alpha}_s x_1 y_c}) + \bar{\alpha}_s \int_{x_c}^{\min(X-x_2^\star, x_0)} dx_1\, R(x_1) e^{2\sqrt{\bar{\alpha}_s x_1 \frac{3}{2}(x_0-x_1)}} \\
&= -1 + \mathrm{I}_0(2\sqrt{\bar{\alpha}_s x_c y_c}) + \bar{\alpha}_s^{1/4} \sqrt{\frac{x_0}{4\pi}} \int_{x_c/x_0}^{\min(1,(X-x_2^\star)/x_0)} \frac{dx_1'}{x_1'^{1/2}} \\
&\qquad \times \left(\frac{3(1-x_1')}{2x_1}\right)^{1/4} e^{2x_0\sqrt{\frac{3}{2}\bar{\alpha}_s x_1'(1-x_1')}} \\
&\overset{\sqrt{\bar{\alpha}_s} x_0 \to \infty}{\sim} \frac{e^{2\sqrt{\bar{\alpha}_s x_c y_c}}}{\sqrt{4\pi\sqrt{\bar{\alpha}_s x_c y_c}}} + \frac{1}{2} e^{\sqrt{\frac{3\bar{\alpha}_s}{2}} x_0}
\end{aligned} \quad \text{(C.8)}$$

The first term in equation (C.8) is subleading due to the square root in the argument and in the denominator. Thus, the leading term for $\mathcal{N}_{\rm med}$ comes from the "inside-medium" region with $\omega_1 \leq \omega_c$.[20]

The saddle point of the integral over x_1 is $x_1^\star = x_0/2 = \ln(\sqrt{p_{T0}/\omega_0(R)})$ so our estimation for $\mathcal{N}_{\rm med}$ is valid only if $x_c < x_1^\star < X - x_2^\star$. The condition $x_c < x_1^\star$ leads to the condition (5.9). The condition $x_1^\star < X - x_2^\star$ leads to the condition (5.10), when $x_2^\star = \ln(\sqrt{\omega_L(\theta)/\omega})$ is evaluated at its largest value, that is when $\theta = \theta_{\rm min} \equiv k_{\perp,\rm min}/\omega$.

We have thus demonstrated that when both $\sqrt{\bar{\alpha}_s} x_0 \equiv \sqrt{\bar{\alpha}_s}\ln(p_{T0}/\omega_0(R))$ and $\sqrt{\bar{\alpha}_s}(X+Y-x_L) \equiv \sqrt{\bar{\alpha}_s}\ln(\omega_L(\theta)/\omega)$ are large and $X > x_1^\star + x_2^\star$, i.e. $\omega < \omega_{\rm cr}$, we have

$$T_{i,\rm out}(X,Y) \sim \frac{\bar{\alpha}_s}{4} \exp\left[\sqrt{\bar{\alpha}_s}\left(X+Y-x_L+\sqrt{\frac{3}{2}}x_0\right)\right], \quad \text{(C.9)}$$

which is precisely formula (5.11).

From (C.9) and (5.5), one deduces the asymptotic DLA behaviour of the small-x fragmentation function by integrating $T_i(\omega, \theta^2 | p_{T0}, R^2)$ over θ^2 between $k_{\perp,\rm min}^2/\omega^2$ and R^2.

[20] That is why we can trust our final result for $T(\omega, \theta^2)$ even for $\theta^2 \leq \theta_c^2$.

JHEP10(2020)204

The leading contribution comes from the lower limit of this integral or, in logarithmic units, from the upper bound $2(x_{\max} - X)$ on the integral on Y, with $x_{\max} = \ln(p_{T0}R/k_{\perp,\min})$. This reproduces (5.12) in logarithmic units:

$$D_i^{\rm med}(X) = \int_0^{2(x_{\max}-X)} {\rm d}Y\, T_i(X,Y) \simeq \frac{\sqrt{\bar\alpha_s}C_i}{4C_A} \exp\left[\sqrt{\bar\alpha_s}\left(-X + 2x_{\max} - x_L + \sqrt{\frac{3}{2}}x_0\right)\right]. \tag{C.10}$$

Finally, the asymptotic form of the ratio $\mathcal{R}_i(X) \equiv D_i^{\rm med}(X)/D_i^{\rm vac}(X)$ is obtained from (C.10) and (5.4), using again the asymptotic form of $\mathrm{I}_1(x)$ at large x:

$$D_i^{\rm vac}(X) \simeq \frac{C_i}{\sqrt{4\pi C_A}}\left[\frac{2\bar\alpha_s(x_{\max}-X)}{X^3}\right]^{1/4} \exp\left(2\sqrt{2\bar\alpha_s X(x_{\max}-X)}\right) \tag{C.11}$$

$$\mathcal{R}_i(X) \sim \frac{\sqrt{\bar\alpha_s\pi}}{2} e^{\sqrt{\frac{3}{2}}x_0 - x_L}\left[\frac{X^3}{2\bar\alpha_s(x_{\max}-X)}\right]^{1/4} \exp\left[\sqrt{\bar\alpha_s}\left(\sqrt{X} - \sqrt{2(x_{\max}-X)}\right)^2\right]. \tag{C.12}$$

From (C.11), one can estimate the position of the maximum $x_{\rm hump}$ of $D_i^{\rm vac}(X)$. Neglecting the non-exponential prefactor, one finds ${\rm d}D_i^{\rm vac}/{\rm d}X \propto x_{\max} - 2X$, so that the $x_{\rm hump} \simeq x_{\max}/2$ and $\omega_{\rm hump} \simeq \sqrt{p_{T0}k_{\perp,\min}/R}$. For $X \geq x_{\rm hump}$ i.e. $\omega \leq \omega_{\rm hump}$, the derivative is negative, hence $D_i^{\rm vac}(\omega)$ decreases when ω decreases. Similarly, one can study the variation of $\mathcal{R}_i(X)$ from the exponential factor alone:

$$\frac{{\rm d}\mathcal{R}_i}{{\rm d}X} \simeq \frac{\bar\alpha_s\sqrt{\pi}}{2} e^{\sqrt{\frac{3}{2}}x_0 - x_L} \frac{\left(\sqrt{2X} + \sqrt{x_{\max}-X}\right)\left(\sqrt{X} - \sqrt{2(x_{\max}-X)}\right)}{\sqrt{X(x_{\max}-X)}} \times e^{\sqrt{\bar\alpha_s}\left(\sqrt{X} - \sqrt{2(x_{\max}-X)}\right)^2}. \tag{C.13}$$

The derivative is positive when $\sqrt{X} - \sqrt{2(x_{\max}-X)} \geq 0$ i.e. when $X \geq 2x_{\max}/3$. Hence, for $\omega \lesssim (p_{T0}k_{\perp,\min}^2/R^2)^{1/3}$, the ratio $R_i(\omega)$ increases when ω decreases.

References

[1] ATLAS collaboration, *Measurement of jet fragmentation in Pb+Pb and pp collisions at* $\sqrt{s_{NN}} = 5.02$ *TeV with the ATLAS detector*, *Phys. Rev. C* **98** (2018) 024908 [arXiv:1805.05424] [INSPIRE].

[2] M. Spousta and B. Cole, *Interpreting single jet measurements in Pb+Pb collisions at the LHC*, *Eur. Phys. J. C* **76** (2016) 50 [arXiv:1504.05169] [INSPIRE].

[3] J. Casalderrey-Solana, D. Gulhan, G. Milhano, D. Pablos and K. Rajagopal, *Angular structure of jet quenching within a hybrid strong/weak coupling model*, *JHEP* **03** (2017) 135 [arXiv:1609.05842] [INSPIRE].

JHEP10(2020)204

[4] Y. Tachibana, N.-B. Chang and G.-Y. Qin, *Full jet in quark-gluon plasma with hydrodynamic medium response*, *Phys. Rev. C* **95** (2017) 044909 [arXiv:1701.07951] [INSPIRE].

[5] R. Kunnawalkam Elayavalli and K.C. Zapp, *Medium response in JEWEL and its impact on jet shape observables in heavy ion collisions*, *JHEP* **07** (2017) 141 [arXiv:1707.01539] [INSPIRE].

[6] W. Chen, S. Cao, T. Luo, L.-G. Pang and X.-N. Wang, *Effects of jet-induced medium excitation in γ-hadron correlation in A+A collisions*, *Phys. Lett. B* **777** (2018) 86 [arXiv:1704.03648] [INSPIRE].

[7] J. Casalderrey-Solana, Z. Hulcher, G. Milhano, D. Pablos and K. Rajagopal, *Simultaneous description of hadron and jet suppression in heavy-ion collisions*, *Phys. Rev. C* **99** (2019) 051901 [arXiv:1808.07386] [INSPIRE].

[8] J. Casalderrey-Solana, G. Milhano, D. Pablos and K. Rajagopal, *Modification of jet substructure in heavy ion collisions as a probe of the resolution length of quark-gluon plasma*, *JHEP* **01** (2020) 044 [arXiv:1907.11248] [INSPIRE].

[9] P. Caucal, E. Iancu, A.H. Mueller and G. Soyez, *Vacuum-like jet fragmentation in a dense QCD medium*, *Phys. Rev. Lett.* **120** (2018) 232001 [arXiv:1801.09703] [INSPIRE].

[10] P. Caucal, E. Iancu and G. Soyez, *Deciphering the z_g distribution in ultrarelativistic heavy ion collisions*, *JHEP* **10** (2019) 273 [arXiv:1907.04866] [INSPIRE].

[11] Y. Mehtar-Tani, C.A. Salgado and K. Tywoniuk, *Anti-angular ordering of gluon radiation in QCD media*, *Phys. Rev. Lett.* **106** (2011) 122002 [arXiv:1009.2965] [INSPIRE].

[12] Y. Mehtar-Tani, C.A. Salgado and K. Tywoniuk, *Jets in QCD media: from color coherence to decoherence*, *Phys. Lett. B* **707** (2012) 156 [arXiv:1102.4317] [INSPIRE].

[13] J. Casalderrey-Solana and E. Iancu, *Interference effects in medium-induced gluon radiation*, *JHEP* **08** (2011) 015 [arXiv:1105.1760] [INSPIRE].

[14] Y. Mehtar-Tani and K. Tywoniuk, *Jet (de)coherence in Pb-Pb collisions at the LHC*, *Phys. Lett. B* **744** (2015) 284 [arXiv:1401.8293] [INSPIRE].

[15] R. Baier, A.H. Mueller, D. Schiff and D.T. Son, *'Bottom up' thermalization in heavy ion collisions*, *Phys. Lett. B* **502** (2001) 51 [hep-ph/0009237] [INSPIRE].

[16] S. Jeon and G.D. Moore, *Energy loss of leading partons in a thermal QCD medium*, *Phys. Rev. C* **71** (2005) 034901 [hep-ph/0309332] [INSPIRE].

[17] J.-P. Blaizot, E. Iancu and Y. Mehtar-Tani, *Medium-induced QCD cascade: democratic branching and wave turbulence*, *Phys. Rev. Lett.* **111** (2013) 052001 [arXiv:1301.6102] [INSPIRE].

[18] J.-P. Blaizot, F. Dominguez, E. Iancu and Y. Mehtar-Tani, *Probabilistic picture for medium-induced jet evolution*, *JHEP* **06** (2014) 075 [arXiv:1311.5823] [INSPIRE].

[19] R. Baier, Y.L. Dokshitzer, A.H. Mueller, S. Peigne and D. Schiff, *Radiative energy loss of high-energy quarks and gluons in a finite volume quark-gluon plasma*, *Nucl. Phys. B* **483** (1997) 291 [hep-ph/9607355] [INSPIRE].

[20] R. Baier, Y.L. Dokshitzer, A.H. Mueller, S. Peigne and D. Schiff, *Radiative energy loss and p_T broadening of high-energy partons in nuclei*, *Nucl. Phys. B* **484** (1997) 265 [hep-ph/9608322] [INSPIRE].

[21] B.G. Zakharov, *Fully quantum treatment of the Landau-Pomeranchuk-Migdal effect in QED and QCD*, *JETP Lett.* **63** (1996) 952 [hep-ph/9607440] [INSPIRE].

JHEP10(2020)204

[22] B.G. Zakharov, *Radiative energy loss of high-energy quarks in finite size nuclear matter and quark-gluon plasma*, *JETP Lett.* **65** (1997) 615 [hep-ph/9704255] [INSPIRE].

[23] R. Baier, Y.L. Dokshitzer, A.H. Mueller and D. Schiff, *Medium induced radiative energy loss: Equivalence between the BDMPS and Zakharov formalisms*, *Nucl. Phys. B* **531** (1998) 403 [hep-ph/9804212] [INSPIRE].

[24] L. Fister and E. Iancu, *Medium-induced jet evolution: wave turbulence and energy loss*, *JHEP* **03** (2015) 082 [arXiv:1409.2010] [INSPIRE].

[25] ATLAS collaboration, *Measurement of the nuclear modification factor for inclusive jets in Pb+Pb collisions at* $\sqrt{s_{\mathrm{NN}}} = 5.02$ *TeV with the ATLAS detector*, *Phys. Lett. B* **790** (2019) 108 [arXiv:1805.05635] [INSPIRE].

[26] M. Cacciari, G.P. Salam and G. Soyez, *The anti-k_t jet clustering algorithm*, *JHEP* **04** (2008) 063 [arXiv:0802.1189] [INSPIRE].

[27] M. Cacciari, G.P. Salam and G. Soyez, *FastJet user manual*, *Eur. Phys. J. C* **72** (2012) 1896 [arXiv:1111.6097] [INSPIRE].

[28] J.G. Milhano and K.C. Zapp, *Origins of the di-jet asymmetry in heavy ion collisions*, *Eur. Phys. J. C* **76** (2016) 288 [arXiv:1512.08107] [INSPIRE].

[29] P.M. Chesler and K. Rajagopal, *On the evolution of jet energy and opening angle in strongly coupled plasma*, *JHEP* **05** (2016) 098 [arXiv:1511.07567] [INSPIRE].

[30] K. Rajagopal, A.V. Sadofyev and W. van der Schee, *Evolution of the jet opening angle distribution in holographic plasma*, *Phys. Rev. Lett.* **116** (2016) 211603 [arXiv:1602.04187] [INSPIRE].

[31] Y.-T. Chien and I. Vitev, *Towards the understanding of jet shapes and cross sections in heavy ion collisions using soft-collinear effective theory*, *JHEP* **05** (2016) 023 [arXiv:1509.07257] [INSPIRE].

[32] S. Catani, L. Trentadue, G. Turnock and B.R. Webber, *Resummation of large logarithms in e^+e^- event shape distributions*, *Nucl. Phys. B* **407** (1993) 3 [INSPIRE].

[33] Y. Mehtar-Tani and K. Tywoniuk, *Radiative energy loss of neighboring subjets*, *Nucl. Phys. A* **979** (2018) 165 [arXiv:1706.06047] [INSPIRE].

[34] Y.L. Dokshitzer, V.A. Khoze, A.H. Mueller and S.I. Troian, *Basics of perturbative QCD*, Ed. Frontieres, Gif-sur-Yvette France (1991).

[35] Y.L. Dokshitzer, G.D. Leder, S. Moretti and B.R. Webber, *Better jet clustering algorithms*, *JHEP* **08** (1997) 001 [hep-ph/9707323] [INSPIRE].

[36] M. Wobisch and T. Wengler, *Hadronization corrections to jet cross-sections in deep inelastic scattering*, in the proceedings of the *Workshop on Monte Carlo Generators for HERA Physics (Plenary Starting Meeting)*, April 27–30, Hamburg, Germany (1998), hep-ph/9907280 [INSPIRE].

[37] S. Catani, Y.L. Dokshitzer, M.H. Seymour and B.R. Webber, *Longitudinally invariant K_t clustering algorithms for hadron hadron collisions*, *Nucl. Phys. B* **406** (1993) 187 [INSPIRE].

[38] C. Frye, A.J. Larkoski, J. Thaler and K. Zhou, *Casimir meets poisson: improved quark/gluon discrimination with counting observables*, *JHEP* **09** (2017) 083 [arXiv:1704.06266] [INSPIRE].

[39] F.A. Dreyer, G.P. Salam and G. Soyez, *The Lund jet plane*, *JHEP* **12** (2018) 064 [arXiv:1807.04758] [INSPIRE].

JHEP10(2020)204

[40] Y. Mehtar-Tani and K. Tywoniuk, *Groomed jets in heavy-ion collisions: sensitivity to medium-induced bremsstrahlung*, *JHEP* **04** (2017) 125 [arXiv:1610.08930] [INSPIRE].

[41] CMS collaboration, *Studies of jet quenching using isolated-photon+jet correlations in PbPb and pp collisions at* $\sqrt{s_{NN}} = 2.76$ *TeV*, *Phys. Lett. B* **718** (2013) 773 [arXiv:1205.0206] [INSPIRE].

[42] CMS collaboration, *Study of Jet Quenching with* $Z +$ *jet Correlations in Pb-Pb and pp Collisions at* $\sqrt{s}_{NN} = 5.02$ TeV, *Phys. Rev. Lett.* **119** (2017) 082301 [arXiv:1702.01060] [INSPIRE].

[43] J. Brewer, J.G. Milhano and J. Thaler, *Sorting out quenched jets*, *Phys. Rev. Lett.* **122** (2019) 222301 [arXiv:1812.05111] [INSPIRE].

[44] CMS collaboration, *Measurement of jet nuclear modification factor in PbPb collisions at* $\sqrt{s_{NN}} = 5.02$ *TeV with CMS*, CMS-PAS-HIN-18-014 (2019).

[45] ALICE collaboration, *Machine learning based jet momentum reconstruction in Pb-Pb collisions measured with the ALICE detector*, in the proceedings of the *2019 European Physical Society Conference on High Energy Physics*, July 10–17, Ghent Belgium (2019), arXiv:1909.01639 [INSPIRE].

[46] D. Pablos, *Jet suppression from a small to intermediate to large radius*, *Phys. Rev. Lett.* **124** (2020) 052301 [arXiv:1907.12301] [INSPIRE].

[47] S. Catani and L. Trentadue, *Resummation of the QCD perturbative series for hard processes*, *Nucl. Phys. B* **327** (1989) 323 [INSPIRE].

[48] T.A. DeGrand, *Structure functions of quarks, gluons, and hadrons in quantum chromodynamics*, *Nucl. Phys. B* **151** (1979) 485.

JHEP10(2020)204